

Lithium-ion batteries for sustainable energy storage: recent advances towards new cell configurations

Daniele Di Lecce^a, Roberta Verrelli^a and Jusef Hassoun^{b*}

^a Sapienza University of Rome, Department of Chemistry, Piazzale Aldo Moro, 5, 00185, Rome, Italy

^b Department of Chemical and Pharmaceutical Sciences, University of Ferrara, Via Fossato di Mortara, 17, 44121, Ferrara, Italy

* Corresponding author: jusef.hassoun@unife.it

Abstract

The recent advances of the lithium-ion battery concept towards the development of sustainable energy storage systems are herein presented. The study reports on new lithium-ion cells, developed over the last few years with the aim of improving the performance and sustainability of the electrochemical energy storage. Alternative chemistries, involving anode, cathode and electrolyte components, are herein recalled in order to provide an overview of state of the art lithium-ion battery systems, with particular care on the cell configurations currently proposed at the laboratory-scale level. Hence, the review highlights the main issues related to full cell assembly, which have been tentatively addressed by limited number of reports, while many recent papers describe material investigation in half-cells, *i.e.*, employing lithium metal anode. The new battery prototypes here described are evaluated in terms of electrochemical performances, cell balance, efficiency and cycling life. Finally, the applicability of these suitable energy storage systems is evaluated in the light of their most promising characteristics, thus outlining a conceivable scenario of new generation, sustainable lithium-ion batteries.

Introduction

The continuous growth of the world population and the industrial and technological development of the society triggered increasing global energy demand, thus leading to serious challenges and environmental issues over the upcoming decades.¹ The massive exploitation of fossil

fuels and consequent emission of CO₂ and pollutants in the atmosphere may actually accelerate the global climate changes.² Therefore, the exploitation of renewable sources, such as solar and wind energy, is attracting relevant attention in order to reduce the greenhouse gas emissions, as recently established within the Paris Agreements of 2016. Energy generated by intrinsically discontinuous and intermittent renewable sources requires efficient storage for grid stability and widespread distribution to be competitive with the currently most used fossil fuels. In this view, the development of rechargeable batteries of high energy and power density, fast cycling rates, long life, and, at the same time, reasonable cost is expected to allow the progressive transition towards environmentally sustainable energy supplies in the near future.³ Furthermore, the large-scale replacement of internal combustion engines with zero-emissions electrified systems (*i.e.*, EVs) may further decrease of greenhouse gases pollution.⁴ Preliminary steps towards these directions have already been moved, with environmental policies becoming established in several countries and encouraging the electromobility through consumer incentives. However, the actual diffusion of the electric vehicles hinges on the development of storage systems of high volumetric and gravimetric energy density and acceptable costs in order to compete with the traditional ones.⁵

Lithium-ion batteries (LIBs), *i.e.*, the most versatile and attracting energy storage systems, have triggered the global scale diffusion of a vast array of portable electronic devices which rapidly became of daily use in the last 25 years³, and still represent the most convincing choice for both electric vehicles and energy storage grids in the upcoming years. Great efforts from both the academia and the industry have been addressed towards the development of a new generation of batteries suitable for emerging applications in terms of gravimetric and volumetric power and energy densities, as well as in terms of sustainability and environmental compatibility.⁶ Accordingly, the LIB chemistry has been gradually improved since the first commercialization in 1991, thus leading to performance matching the requirements of new technologies. In the mid-1990s the most diffuse LIBs employed a graphite anode, an electrolyte based on lithium salt and carbonate solvents and a LiCoO₂ cathode, resulting in a gravimetric energy density of about 190 Wh kg⁻¹.⁷ Conventional C/LiCoO₂ cell bears

several intrinsic limitations, including i) the relatively limited intercalation ability of graphite (*i.e.*, of about 0.17 moles of Li per mole of Carbon); ii) the high cost and environmental issues posed by the use of Co; iii) the low thermal stability of the $\text{Li}_{1-x}\text{CoO}_2$ phase formed during charge.^{8,9} The C/LiFePO₄ configuration was introduced in the early 2000s in order to decrease the cost and toxicity of the battery.⁷ However, the relatively low operating voltage of the cathode (*i.e.*, 3.45 V *vs* Li⁺/Li), affected the energy density of the battery. Technological upgrade, optimization of conventional cells' design as well as exploitation of alternative electrode chemistries so far represented the most explored strategies for increasing the energy density achieved by the battery.^{10,11} Beside cell technology optimization, the development of new anode, cathode and electrolyte materials of enhanced performances attracted great efforts and recently increasing funds. Among the alternative anodes, alloying materials such as Sn or Si and metal oxide conversion materials, reversibly exchanging more than 1 mol of Li⁺ for mol of active specie, appear optimal candidates to achieve high specific capacities.¹²⁻¹⁶ Sn and Si electrodes, which bear the additional advantage of being naturally abundant, have already been optimized up to the market level.¹⁷ Possible alternative to conventional graphite anode employed in several full cells and characterized by very high safety content is represented by Lithium Titanium Oxide ($\text{Li}_4\text{Ti}_5\text{O}_{12}$).¹⁶ This anode is characterized by high thermal stability and operates at 1.5 V *vs* Li⁺/Li, thus avoiding lithium plating upon charge. The material cycles by very fast rate with a specific capacity of 170 mAh g⁻¹.¹⁸

As for the cathode side, the research is mostly focusing on materials characterized by lower cost and toxicity with respect to LiCoO₂, as well as by higher specific capacity and/or working voltage in order to increase the battery energy density. Accordingly, LiCoO₂ has been efficiently replaced by other families of layered compounds, namely $\text{LiNi}_{1/3}\text{Mn}_{1/3}\text{Co}_{1/3}\text{O}_2$ (NMC) and $\text{LiNi}_{0.8}\text{Co}_{0.15}\text{Al}_{0.05}\text{O}_2$ (NCA), which have lower Co content than LiCoO₂, average operating voltage of about 3.7 V *vs* Li⁺/Li, higher reversible capacity (about 180 – 185 mAh g⁻¹) and the additional advantage of higher thermal stability in their de-lithiated form.^{8,19,20} These cathode materials have been successfully launched onto the market and are currently employed in commercial LIBs.⁷ Furthermore, great

attention is now devoted to Li-rich layered compounds, generally described by the chemical formula $(1-x)\text{Li}_2\text{MnO}_3 \cdot x\text{LiMO}_2$ (where $M = \text{Co}, \text{Mn}, \text{Ni}$ and Li/M ratio > 1).²¹ Despite their remarkable capacity, *i.e.*, exceeding 200 mAh g^{-1} and the advantage represented by the high manganese content, these materials need further optimization in order to overcome the issues of structural instability, voltage hysteresis and decay upon prolonged cycling.⁸ LiFePO_4 olivine is a low cost and environmentally friendly cathode already used in commercial LIBs,²² as above mentioned, which is characterized by remarkable chemical and electrochemical stability with respect to the layered-structure materials.²³ A vast array of polyanionic olivines characterized by higher working voltage than LiFePO_4 , such as $\text{LiFe}_{0.5}\text{Mn}_{0.5}\text{PO}_4$ and LiCoPO_4 , has been recently investigated as viable cathodes for next generation batteries. These materials have higher theoretical energy density compared to LiFePO_4 .²⁴ In particular, LiCoPO_4 exchanges Li^+ ions at potential *vs* Li^+/Li as high as 4.8 V ,²⁵ however it is characterized by expected high cost and environmental concerns due to cobalt. A very interesting class of Co-free cathode materials suitable for high energy LIB batteries is represented by spinel-structured electrodes, such as LiMn_2O_4 and $\text{LiNi}_{0.5}\text{Mn}_{1.5}\text{O}_4$, working at about 4.1 and $4.7 \text{ V vs Li}^+/\text{Li}$, respectively.^{26,27}

Beyond conventional insertion cathodes, the exploitation of Li/O_2 and Li/S battery systems, exhibiting much higher theoretical energy densities, may provide a real breakthrough in terms of battery performances and sustainability.^{1,9,28,29} These challenging fields of research are continuously expanding over recent years: Li/O_2 batteries are still at a research level and may be practically employed only by middle- to long-term perspective, while the recent progress achieved for Li/S batteries holds the promise for their large-scale diffusion in the near future.

The increase of LIB performances, targeted in order to achieve satisfactory high energy density, implies the use of very stable electrolyte solutions for ensuring cell safety and lifetime. Within the challenging research field of next generation LIBs' electrolytes, several viable alternatives have been suggested, such as ionic liquids (ILs), which are considered "green" and sustainable alternatives to conventional electrolytes, as indeed demonstrated by several proof-of-concept battery

prototypes exhibiting remarkable performances.³⁰ Solvents, co-solvents and electrolyte additives have been intensively studied and optimized for achieving electrolyte solution with optimized characteristics.^{31,32} Moreover, polymer and solid electrolytes have attracted increasing attention over the years, revealing promising features for the development of highly safe lithium and lithium-ion batteries.^{17,33,34} Several fluorine-free salts have been developed and studied in order to further decrease the toxicity and hazards of the cell.³⁵

Relevant efforts have been devoted towards the reduction of the costs and environmental impact of the electrode materials (synthesis and processing) as well as to the development of efficient and sustainable battery recycling methodologies.^{1,36} In this respect, the attention has been mainly focused on the recovery of the valuable Co, Li and Mn metals from spent LIBs through combined mechanical and chemical treatments. The optimization of the recovery and recycling process of spent batteries through environmentally friendly routes (such as the bioleaching) is expected to further enhance the overall sustainability of Li-Ion energy storage systems.³⁶

Furthermore, concerns over the geographical availability and cost of lithium metal have recently triggered the study and development of a “post-lithium” battery technology, based on more naturally abundant elements such as Na, Ca, Mg, K, Al, etc.^{37,38} Beside sodium, several open challenges still hamper the practical exploitation of Ca, Mg, K and Al battery technologies.³⁷ Moreover, batteries employing organic electrode materials are now emerging as very promising and “green” alternatives to conventional inorganic battery systems; however their development is still at a preliminary research level.³⁹

This review aims to shed light on the most recent advances of the LIB concept towards the development of high-performance energy storage systems. In particular, the attention is focused on new LIB prototypes, suggested over the last few years as viable and sustainable alternatives to conventional cell configurations. A vast array of laboratory-scale and proof-of-concept batteries is herein critically discussed, highlighting the main advantages and drawbacks of the various configurations. Battery suitability for practical applications is herein rationalized by focusing the

attention on the electrochemical behavior under operating conditions of full lithium-ion cells combining novel anodes, cathodes and electrolytes. We recall several examples of LIBs prototypes to discuss the critical issues associated to the full cell assembly and test, including the selection of optimal cathode/anode mass ratio and voltage limits. Particular attention is devoted to the role of the overall full cell balance for achieving prolonged battery stability, voltage retention, and for avoiding active material losses due to parasitic reactions, which may continuously modify the anode/cathode ratio over cycling.⁴⁰ The review includes four main sections according to the type of employed cathode, since the voltage, expected cost and environmental impact of the full cell strongly hinge on the positive electrode features. Thus, LIB prototypes using layered oxides, phospho-olivines, spinel oxides, as well as sulfur- and oxygen-based cathodes are reported and discussed individually. In particular, in the first section, the review surveys high-performance batteries based on LiCoO_2 materials, *i.e.*, the conventional cathode, and new cells employing layered oxides in which Co is partially substituted by Mn, Ni and Al, and preliminary examples of LIBs based on high-capacity Li-rich materials. The second section focuses the attention on batteries using polyanionic LiFePO_4 olivine, which has demonstrated relevant performance in terms of stability and cycling life, as well as on recent attempts to increase the cell energy density by Fe substitution in the $\text{LiFe}_{1-x}\text{MePO}_4$ cathode. The increase of stored energy by use of high-voltage cathodes is further discussed in the third section, which deals with new LIBs having spinel oxides as the positive electrode. The design of high-performance battery configurations through optimal electrode formulation and material engineering, the use of nano-architectures, the optimization of active materials morphology and particle size, and the use of composite electrodes, are covered by the sections. Hence, the fourth section of the Review reports on lithium-ion batteries employing sulfur and oxygen cathodes, which represent a new attractive choice for the future development of an advanced and sustainable energy storage technology, with particular environmental and economic advantages. This section demonstrates the possible use of sulfur-based cathodes in lithium-ion cells with relevant

performances and reveals the main issues currently affecting metal-free oxygen batteries shown by preliminary results.

According to the above description, Scheme 1 represents a flow chart including key principles and guidelines throughout the survey of the LIB battery prototypes reported in this Review.

Scheme 1

Therefore, this paper highlights the crucial role of full cell prototype studies for demonstrating the applicability at laboratory scale of recently proposed cathode, anode and electrolyte materials. In particular, the critical analysis of LIBs covered by this review may be of definite interest in order to outline the open challenges towards the achievement of a sustainable, advanced energy storage technology in the next future.

1. Lithium-ion batteries using layered cathodes

Layered-structure cathodes, among which the most known is LiCoO_2 (*i.e.*, LCO), currently represent the cathode materials of use in combination with graphite anode.^{8,9} Various configurations of layered cathodes, in which cobalt is partially replaced by nickel/manganese (NMC) or nickel/aluminum (NCA) were reported to have operating voltage of 3.8 V, specific capacities exceeding 200 mAh g^{-1} and excellent rate capability, *i.e.*, suitable characteristics for emerging applications such as electric vehicles.^{8,19-21} Furthermore, LIBs employing layered cathode materials and carbonaceous anode materials alternative to graphite, such as exfoliated graphite/graphene, have been widely investigated with remarkable results.⁴¹⁻⁴⁵ Great attention has been also focused on the use of unconventional composite anodes based on alloys⁴⁶⁻⁵², titanates⁵³⁻⁵⁷ and metal oxides⁵⁸⁻⁶⁴ for application in new configuration LIBs. Many recent literature works investigated renewed LIBs using a benchmark, even commercial, LCO cathode. Despite these cells often revealed remarkable improvement at the anode side, they suffer from the drawbacks associated with Co-based layered oxide cathode which were previously discussed. Though, these studies may actually facilitate the

evaluation of the anode improvement, thus allowing further enhancement of the full cell features by using a new-generation layered cathodes, such as NMC, NCA and Li-rich oxides.

Accordingly, alloy-based anodes have demonstrated good performances in combination with LCO cathode. Nanocrystalline Si (c-Si) dispersed in amorphous Si (a-Si) encapsulating hard carbon (HC) derived from natural polysaccharide (HC@c-Si@a-Si) was studied in a full cell in combination with LCO.⁶⁵ Despite the use of such an environmentally friendly precursor for the hard carbon synthesis, a further carbon coating via thermal decomposition of acetylene was necessary to enhance the electronic conductivity and form the C-Si phase. The HC@c-Si@a-Si/LCO full cell showed excellent rate capability and very stable, long-term cycle life. The battery exhibited a capacity retention at a rate as high as 10C of 50.8% with respect to the capacity delivered at 1C rate, and of 80% after 160 cycles at 1C rate.

One-pot decoration of Si anode and LCO cathode with colloidal nanoparticles composed of electroconductive antimony-doped tin oxide (ATO) actually enhanced the electronic conduction of the materials and mitigated unwanted interfacial side reactions between electrodes and electrolyte. Thus, a full ATO-Si/ATO-LCO cell was cycled within 2.5 V and 4.4 V, with remarkable volumetric energy density (discharge capacity = 274 mAh cm⁻³) and capacity retention (83.9% upon 100 cycles).⁶⁶ However, the use Sb, even in low amount, further affects the environmental compatibility of the cell.⁶⁷ Moreover, both cathode and anode synthesis involve high temperature solid-state annealing.

A Si-graphene/LCO cell reached volumetric energy densities of 972 and 700 Wh l⁻¹ at the first and 200th cycle, respectively, 1.8 and 1.5 times higher than those of current commercial lithium-ion batteries.⁶⁸ The anode was prepared by directly growing graphene over silicon nanoparticles without silicon carbide formation. This synthesis approach requires heating at high temperature (1000 °C) under CH₄ and H₂; therefore, it is expected to significantly affect the material cost for large-scale production. The graphene layers anchored onto the silicon surface accommodate the volume

expansion of silicon associated with the Li-alloying via a sliding process between adjacent graphene layers.

Three-dimensional (3D) nanoarchitecture of Ge coated with carbon (3D-Ge-C) showed excellent electrochemical performance, hence it was studied in full cell in combination with a LCO cathode.⁶⁹ Upon anode pre-lithiation, the 3D-Ge-C/LCO cell exhibited charge and discharge capacities of 1901 and 1561 mAh g⁻¹, respectively, referred to the 3D-Ge-C mass, initial Coulombic efficiency of about 82.1%, outstanding rate capability, and a retention of 94.7% over 50 cycles. The possible application of LIB prototype was also demonstrated by lighting up a 50-LED bulb array.⁶⁹ The anode was prepared by a facile carbothermal reduction of nano GeO₂ using polyvinylpyrrolidone as precursor. It is noteworthy that germanium is a relatively nontoxic element that poses negligible threat to the environment.⁷⁰

A very interesting LIB array is represented by the combination of LCO cathode and LTO anode. A flexible LIB using the above mentioned configuration, with reinforced electrode design in order to support the active layers of the battery and a freestanding carbon nanotube (CNT) as the current collector (**Fig. 1a**), showed remarkable performances.⁷¹ The CNT layer was prepared by spray painting on a stainless steel foil, while the active materials were embedded inside a porous membrane composed of non-woven fibers. The embedding process was performed by dipping the membrane into an ink bath. Then, the CNT layer was transferred from the stainless steel foil to embedded membrane by simple dipping in water bath. This approach led to electrode tensile strength of one order of magnitude higher than standard electrodes. The freestanding CNT based current collector minimized the thickness of inactive components within the battery. This particular architecture led to areal-capacity enhancement and improved the tensile strength and mechanical flexibility of the electrodes. The cell delivered areal capacity of about 1 mAh cm⁻², *i.e.*, a value 3–4 times higher than other reports on flexible lithium-ion batteries using LTO and LCO electrodes, and a capacity retention of around 94% after cycling the battery for 450 cycles at a C/2 rate (**Fig. 1b**). Tests at different current rates (**Fig. 1c,d**) showed reversible capacity of about 117, 104, and 90 mAh g⁻¹ at C/4, C/2, and 1C

rates, respectively. Furthermore, the reinforced electrode allowed excellent capacity retention after repeatedly flexing to a bending radius ranging from 45 to 10 mm.

Figure 1⁷¹

Flexible LIBs were also reported by using Fe₂N and MoO₂ anodes in combination with LCO cathode.^{72,73} Binder-free Fe₂N nanoparticles (Fe₂N NPs) revealed excellent performance within flexible Fe₂N/LCO configuration battery. The Fe₂N NPs were prepared by hydrothermal treatment followed by annealing at 600 °C in NH₃ gas flow.⁷² The full cell achieved high power density (3200W kg⁻¹) by operating at current density as high as 1000 mA g⁻¹ and high energy density (688 Wh kg⁻¹) at lower current (200 mA g⁻¹). Uniform MoO₂ nanoparticle material, evaluated as intercalation-type lithium anode within the potential window of 1.0 – 2.5 V, showed comparable electrochemical behavior and higher capacity with respect to commercial Li₄Ti₅O₁₂ in half cell, and were therefore employed in a full LIB with LCO cathode. The anode was synthesized by simple hydrothermal pathway followed by annealing at 420 °C in H₂/Ar atmosphere.⁷³ The MoO₂/LCO cell delivered high energy density based on total mass of cathode and anode active materials (179 Wh kg⁻¹), and capacity retention of 87% of the initial capacity after 500 cycles at 1 C rate.

A very interesting LIB, using commercial LCO cathode and a composite, core–shell nanowire anode based on TiO₂-MoO₃ (TO-MO mass ratio 1:1) is reported in **Fig. 2**.⁷⁴ The nanostructured anode (**Fig. 2a,b**), prepared through hydrothermal approach followed by controlled electrodeposition process, was constituted by nano-MoO₃ shell, which provided large specific capacity and high electrical conductivity, and electrochemically stable TiO₂ nanowire core, which ensured negligible volume change during Li⁺ insertion/desertion. Accordingly, the stable TiO₂ core mitigated the cycling instability of MoO₃ shell and its array further provided a 3D scaffold for the electrodeposition of MoO₃. The full-cell (**Fig. 2c**) showed outstanding performance (**Fig. 2d-f**), with maximum power density of 1086 W kg_{total}⁻¹ (based on the total mass of the TO-MO and LiCoO₂) and excellent energy density (285 Wh kg_{total}⁻¹), *i.e.*, a high value with respect to several LIBs previously reported with metal oxide anode. However, it is worth considering that molybdenum is not an abundant element

and is mostly produced as byproduct of copper mining and in less amount from primary ore. Therefore, its use in LIBs may further decrease the environmental compatibility of this type of cells. Furthermore, the Mo price is sensitive to the copper production.⁷⁵

Figure 2⁷⁴

A relevant class of energy storage systems with high energy content is represented by LIBs combining NMC or NCA cathodes with carbonaceous,^{76–80} alloy,^{81–85} titanates,^{86,87} oxides^{88,89} and sulfites.⁹⁰ Partial substitution of Mn, Ni, and Al for Co within the layered cathode structure may improve thermal stability and reversible capacity of the cell, as well as decrease its cost and environmental concerns. It is worth mentioning that limited content of Co and Ni within the layered structure may further enhance the battery sustainability.⁹¹ Among the studied cell configurations, porous carbon–Fe₃O₄/Li[Ni_{0.59}Co_{0.16}Mn_{0.25}]O₂ full cell exhibited high areal and gravimetric capacities (748 mAh cm⁻² and 150 mAh g⁻¹, respectively) at about 3.2 V, which led to a theoretical energy density of 483 Wh kg⁻¹ with respect to the cathode weight.⁹² The cathode powder was prepared by coprecipitation method followed by high-temperature treatment (850 °C) under oxygen, while the anode was synthesized by sol-gel approach with annealing (500°C) in Ar atmosphere. The battery reversibly operated within 50 and 800 mA g⁻² current, with a retention of 63.8% after 1000 cycles at 0.505 mA (*i.e.*, 50 mA g⁻² with respect to the cathode). A bifunctional nanostructured anode based on selenium/micro–mesoporous carbon sphere (Se-MPCS) was successfully employed in a LIB with LiNi_{1/3}Mn_{1/3}Co_{1/3}O₂ cathode.⁹³ Se-MPCS was prepared by introducing Se into a carbon matrix through heating a mixture of Se powder and carbon at 240 °C. The carbon host was synthesized by a low-temperature hydrothermal process. Furthermore, the negative electrode layers were prepared by a sustainable aqueous process employing carboxymethyl cellulose (CMC) and styrene butadiene rubber (SBR). The full Se-MPCS/NMC cell showed at a rate of 1C a reversible capacity of 110 mA h g⁻¹ based on the cathode mass, with a Coulombic efficiency of approximately 100%, and retained 80% and 50% of the initial reversible capacity after 500 and 1000 cycles, respectively. A very stable and safe LIB employed a Pyr₁₄TFSI-LiTFSI non-flammable ionic liquid (IL) electrolyte, a

nanostructured Sn-C nanocomposite anode prepared by sol-gel approach and a commercial layered NMC cathode (**Fig. 3**).⁹⁴ The anode was synthesized by heating at 700 °C under Ar flow a resorcinol-formaldehyde gel infiltrated by an organometallic Sn precursor. The battery had outstanding characteristics in terms of cycle life, efficiency, optimal electrodes/electrolyte interface features and energy density (see **Fig. 3a-c**). The electrolyte ensured conductivity value varying from about 2 mS cm⁻¹ at 40 °C to 7 mS cm⁻¹ at 60 °C, and viscosity ranging from 144 mPa s at 20 °C to 27 mPa s at 60 °C, *i.e.*, suitable values for battery application. The use of the Sn-C nanocomposite anode and the NMC layered cathode, having a remarkable structural integrity demonstrated by the EIS/SEM study (**Fig. 3c**), guaranteed rather high cell energy density and long-term stability. Indeed, the cell was characterized by a reversible capacity referred to the cathode mass of about 140 mAh g⁻¹ and an average working voltage of about 3.4 V, thus leading to theoretical energy density of approximately 476 Wh kg⁻¹ as referred to the cathode. This value reflected practical energy density exceeding 200 Wh kg⁻¹. Furthermore, the cell showed stability exceeding 400 galvanostatic cycles, high efficiency and capacity retention approaching 100 %.

Figure 3⁹⁴

The surface reactivity of layered cathodes plays a crucial role in the electrochemical behavior of the cell. Therefore, mixed oxides having concentration gradient of the transition metal ions from the particle core to the outer layer revealed at the same time relevant energy density and enhanced cycling stability, due to the improvement of the electrode/electrolyte interface. Accordingly, nanostructured layered material based on lithium–nickel–manganese–cobalt oxide, where the manganese concentration remained constant throughout the particle, while the nickel concentration decreased and the cobalt concentration increased linearly from the particle center to the surface, has been reported as new, high performance cathode for LIBs (see **Fig. 4a-b**).⁹⁵ The synthesis was carried out by using two continuously stirred tank reactors containing two aqueous solutions of Ni, Co, and Mn of different concentration. After coprecipitation, the obtained precursor was mixed with LiOH

and calcined at 850 °C in air. The resulting material had average composition of $\text{Li}[\text{Ni}_{0.60}\text{Co}_{0.15}\text{Mn}_{0.25}]\text{O}_2$ and was composed of rod-shaped primary particles grown in radial directions with crystallographic texture. This particular morphology ensured high rate capability, increased the low temperature performance, and improved the thermal stability compared to a benchmark cathode having the same composition and fixed transition metal concentration. The electrode was tested in full pouch cell (35 mAh) with MCMB graphite anode between 3.0 V and 4.4 V at 25 °C and 55 °C with a specific current of 195 mA g⁻¹ (1C = 180 mA g⁻¹). The cell revealed good capacity retention (70.3%) after 1000 cycles, even at 55 °C (**Fig. 4c-d**).⁹⁵ Following the same approach, a recent paper reported concentration-gradient Ni-rich layered oxide electrode with an average composition of $\text{LiNi}_{0.76}\text{Co}_{0.1}\text{Mn}_{0.14}\text{O}_2$.⁹⁶ Also in this case, the nickel content decreased gradually and the manganese content increased linearly from the center to the surface of each particle (**Fig. 4e**). The material was prepared by a three-step coprecipitation method using a tank reactor, followed by lithiation process and thermal treatment at 750 °C in oxygen atmosphere. Compared to a constant-concentration sample, the gradient sample exhibited higher reversible capacity with superior cycling properties in half-cell, as a consequence of the higher content of inactive tetravalent Mn on the surface suppressing the reaction with the electrolyte (**Fig. 4e**). The improved cathode was employed in a pouch-type full cell with a graphite anode, which delivered a capacity as high as 19.6 mAh and a retention of 89% upon 500 cycles at C/3 rate (1C = 200 mA g⁻¹, **Fig. 4f**). Furthermore, $\text{Li}[\text{Ni}_{0.75}\text{Co}_{0.1}\text{Mn}_{0.15}]\text{O}_2$ cathode with Ni-rich core and a Ni-depleted shell and continuous concentration gradient between the core and shell was used in a LIB with high capacity Si-C composite anode, internally wired with graphene sheets (IWGS, about 6 wt% of graphene). The anode was prepared by a scalable sol-gel process in water followed by annealing at 850 °C in inert atmosphere.⁹⁷ The battery operated within the 3.2 – 4.2 V range with specific capacity per cathode mass of 200 mAh g⁻¹ and 170 mAh g⁻¹ at 0.1C and 1C rates, respectively. Therefore, the cell was characterized by excellent cycling stability up to 750 cycles at 1C rate, a theoretical energy density as high as 720 Wh kg⁻¹, and an estimated practical energy density higher than 240 Wh kg⁻¹.

Figure 4^{95,96}

A very recent class of materials belonging the layered oxide-structure is the Li-rich family, characterized by the composition of $x\text{Li}_2\text{MnO}_3 \cdot (1-x)\text{LiNi}_a\text{Co}_b\text{Mn}_c\text{O}_2$ (where $a + b + c = 1$). These materials have gained extensive attention due to their remarkable reversible capacity, *i.e.*, higher than 250 mAh g^{-1} . However, only a few paper reported on their application in full LIB. The synthesis and application in LIB using graphite anode of a $x\text{Li}_2\text{MnO}_3 \cdot (1-x)\text{LiNi}_{0.7}\text{Co}_{0.15}\text{Mn}_{0.15}\text{O}_2$ ($x = 0, 0.03, 0.07, 0.10, 0.20, \text{ and } 0.30$) cathodes, which combine the advantages of the high specific capacity of Ni-rich layered phase and the surface chemical stability of Li-rich layered phase materials, has been recently reported.⁹⁸ Interestingly, the material was prepared by simple grinding of a $\text{Ni}_{0.7}\text{Co}_{0.15}\text{Mn}_{0.15}(\text{OH})_2$ precursor with MnCO_3 and LiOH , followed by heating at $800 \text{ }^\circ\text{C}$. The $\text{Ni}_{0.7}\text{Co}_{0.15}\text{Mn}_{0.15}(\text{OH})_2$ precursor was synthesized by using a continuous stirring tank reactor. **Fig. 5** shows standard and cross section electron micrographs (left panels) as well as SEM-EDS line scans (right panels) of the resulting $x\text{Li}_2\text{MnO}_3 \cdot (1-x)\text{LiNi}_{0.7}\text{Co}_{0.15}\text{Mn}_{0.15}\text{O}_2$ particles with $x = 0$ (panels a) and $x = 0.10$ (panels b). Deep electrode characterization by X-ray diffraction, electron microscopy and electrochemical measurements confirmed the formation of a Li-rich layered phase with $C2/m$ symmetry and revealed Li-rich nano-domain islands embedded into the conventional Ni-rich layered matrix ($R\bar{3}m$), as shown by the scheme of **Fig. 5c**, right panel. Remarkably, a pouch-type LIB using the optimized cathode material ($x=0.07$) and graphite anode revealed an initial capacity of 190 mA h g^{-1} , retained by 74% after 900 cycles (**Fig. 5d**).⁹⁸ Further LIBs using Li-rich cathode in combination with graphite anode, such as SnO_2 -coated $\text{Li}_{1.2}\text{Mn}_{0.54}\text{Co}_{0.13}\text{Ni}_{0.13}\text{O}_2$ (with reversible capacity of about 230 mAh g^{-1} retained by 87% over 150 cycles in full cell⁹⁹) and Ti-substituted $0.5\text{Li}_2\text{MnO}_3\text{-}0.5\text{LiNi}_{0.5}\text{Mn}_{0.5}\text{O}_2$ cathode with the composition of $\text{Li}_{1.5}\text{Ni}_{0.25}\text{Mn}_{0.75-x}\text{Ti}_x\text{O}_{2.5}$,¹⁰⁰ have been recently reported.

Figure 5⁹⁸

2. Lithium-ion batteries using olivine cathodes

Olivine materials, in particular LiFePO_4 , are the most stable and long-life cathodes designed for LIBs application. Furthermore, those based on manganese and iron are particularly appealing because of the low cost and environmental compatibility with respect to Co and Ni-based materials.¹ LiFePO_4 (*i.e.*, LFP) can be efficiently employed in several LIB configurations using carbonaceous anodes. An interesting example is the flexible graphite/LFP battery integrated into a single paper structure, using nano-fibrillated cellulose both as electrode binder material and as separator material.¹⁰¹ The battery papers are made through a paper-making type process by sequential filtration of water dispersions containing the battery components. This process ensured a thin and robust paper cell. It is noteworthy that commercial Li-ion batteries employ separators based on polyethylene–polypropylene, which are synthesized from non-renewable petroleum products. As for conventional binders, they are F-containing polymers that require coating process in organic toxic solvents. Therefore, the use of cellulose-based polymers is expected to significantly improve the environmental compatibility of the battery. The paper cell delivered reversible capacities of 146 mAh g^{-1} and 101 mAh g^{-1} with respect to the cathode mass at C/10 and 1 C rates, respectively. The corresponding energy density at C/10 rate was 188 Wh kg^{-1} .

An interesting lithium-ion cell characterized by relevant safety content was formed by coupling LFP cathode with a graphene nanoplatelet (GNP) anode prepared by an easy-to-handle aqueous ink cast on copper foil, in N-butyl-N-methyl-pyrrolidinium-bis (trifluoromethanesulfonyl) imide, lithium bis(trifluoromethanesulfonyl)imide, ethylene carbonate, dimethyl carbonate ($\text{Pyr}_{1,4}\text{TFSI-LiTFSI-EC-DMC}$) electrolyte.¹⁰² The GNP/LFP battery delivered a capacity of the order of 150 mAh g^{-1} at 2.4 V, with an efficiency approaching 100%.

Another example of cell based on Cu-supported graphene nanoflakes anode and LFP has been reported as low cost and potentially scalable battery.¹⁰³ A graphene nanoflakes ink was prepared by easy exfoliation via ultrasonication in N-methyl-2-pyrrolidone. The lithium-ion cell achieved optimal performances by carefully balancing its composition and suppressing the initial irreversible capacity of the anode in the round of few cycles. The cell delivered specific capacity of 165 mAh g^{-1} at 1C rate

for over 80 cycles with Coulombic efficiency approaching 100%. The related theoretical energy density was 380 Wh kg^{-1} , with estimated energy density of about 190 Wh kg^{-1} . The good performance and the use of low cost and environmentally friendly materials make this cell configuration an interesting candidate for the development of sustainable batteries. However, the relatively large voltage slope of graphite/graphene materials may be an issue for practical applications. Other recent studies reported the use of carbonaceous anode materials in combination with LFP cathodes with promising results.^{45,104–107}

Several advantages in terms of cycle life and safety content may be achieved by using LFP in combination with titanium oxide based anodes, *e.g.*, TiO_2 and $\text{Li}_4\text{Ti}_5\text{O}_{12}$ (LTO). Furthermore, titanium is the ninth most abundant element in the Earth's crust and Ti-based oxides are environmentally benign.¹⁰⁸ Hence, LTO/LFP batteries are particularly appealing as sustainable and safe energy storage systems. However, the relatively high and low voltages of Ti-based anode and LFP cathode, respectively, strongly affect the energy density of the cell. A LFP/C cathode networked with MWCNT of enhanced charge mobility was employed in a lithium-ion full cell using $\text{Li}_4\text{Ti}_5\text{O}_{12}$ anode, with working voltage of about 1.9 V, and stable behavior upon 100 cycles.¹⁰⁹ $\text{Li}_4\text{Ti}_5\text{O}_{12}$ nanopowder was synthesized by a solution–combustion synthesis using titanyl nitrate [$\text{TiO}(\text{NO}_3)_2$], LiNO_3 and glycine, while LiFePO_4 particles of about 20 nm were prepared through a sol–gel route employing adipic acid and then added with MWCNT in order to improve the electronic conductivity. An example of LFP-based battery using anatase TiO_2 delivered a reversible capacity of 103 mAh g^{-1} at about 1.4 V, excellent cycling response at several current densities and capacity retention of 88% over 300 cycles in ambient conditions.¹¹⁰ The cell employed TiO_2 hollow nanofibers prepared by simple co-axial electrospinning route and commercial LFP powder. Furthermore, a V-doped $\text{Li}_4\text{Ti}_5\text{O}_{12}$ -C composite material, prepared by high-temperature solid-state method, demonstrated high rate capability and cycling stability.¹¹¹ The V-doped LTO-C/LFP full cell, limited at the anode, delivered discharge capacities of 181, 178, 167, 142, 110, and 78 mAh g^{-1} at 0.2, 0.5, 1, 3, 5, and 10C rates, respectively. The cell had excellent long-term stability upon 400 cycles, with a fading rate lower

than 0.0056% per cycle. Despite the suitable performances, the use of vanadium represents an issue in terms of safety and toxicity of the starting materials.¹¹²

Relevant volumetric and gravimetric energy densities, in addition to low cost, easy synthesis methodologies, high power densities and long cycle life are key requirements for high-performances LIBs. However, too large tap density generally compromises the charge transport and hence the power density. This issue has been recently addressed by using densely packed $\text{Li}_4\text{Ti}_5\text{O}_{12}$ (LTO) submicrospheres, synthesized through a simple and easily scalable self-assembly process, ensuring at the same time high tap density, stable trend, long life and high rate capability.¹¹³ Indeed, compact LTO spheres were formed through hydrolysis reaction followed by annealing in Ar atmosphere. The abundant presence of grain boundaries between the LTO nanocrystallites in the submicron spheres led to a 3D interconnected network, which allowed fast Li-ion and electron transport, as indicated by large Li-ion diffusion coefficient and electronic conductivity values ($6.2 \times 10^{-12} \text{ cm}^2 \text{ s}^{-1}$ at 52% state of charge and $3.8 \times 10^{-6} \text{ S cm}^{-1}$, respectively). The specific capacity for densely packed LTO was reported within the 150 – 130 mAh g^{-1} range at high current rates (10 and 20C), with capacity retention of about 97% after 500 cycles at 10C rate in lithium half-cell. The high-performance anode was combined with commercial LFP cathode in full pouch cell (Fig 1 a,b). The LTO/LFP LIB delivered capacity values of 146, 129, 125, 110, 90, and 76 mAh g^{-1} at 0.5, 5, 10, 30, 60, and 80C rates (Fig. 6c,d). The cell had excellent cycling stability, without capacity decay over 8000 cycles at 30 C rate (Fig. 6e).¹¹³ Further proofs of the efficient use of Ti-based anodes and LFP cathodes in full cells characterized by relevant stability were reported in literature.^{57,114–117}

Figure 6¹¹³

Interestingly, self-supported carbon nanofiber paper (CNFP)-sulfur composite, generally employed as the cathode in lithium metal sulfur battery, was used as the anode in a CNFP-S/LFP LIB with average working voltage of 3.0 V.¹¹⁸ A carbon nanofibers paper was firstly prepared through electrospinning of polyacrylonitrile followed by carbonization at 1000 °C and then infiltrated by sulfur. The reversible Li-ion storage ability of sulfur below 1.5 V vs. Li/Li⁺ in the CNFP matrix,

apparently in contrast to the typical conversion reaction of sulfur to Li_2S within 3.0 – 1.5 V vs. Li/Li^+ potential range, was attributed to the rapid adsorption/desorption of Li -ions on the surface of sulfur. The cell delivered a reversible capacity of about 310 mAh g^{-1} with respect to the total mass of the electrode components, maintaining 95% of capacity after 1000 cycles and exhibiting higher power capability with respect to similar cells based on graphite anode.¹¹⁸ Furthermore, the proposed configuration benefits from the low cost and sustainability of both S-based anode and LFP cathode. Metal oxide anode have been efficiently used in combination with LFP cathode. A recent work¹¹⁹ reported an all-nanosheet LIB employing a ZnMn_2O_4 -graphene anode and a LiFePO_4 cathode, characterized by short Li -ion diffusion length and easy charge transport due to the use of nanostructured electrodes (**Fig. 7a**). Indeed, both electrodes had 2-dimensional (2D) nanosheet morphology which enabled operation at high current (**Fig. 7c**). Indeed, comparison of the electrochemical performances of the all-nanosheet battery with those of a benchmark one using conventional graphite anode and commercial LiFePO_4 cathode revealed superior rate capability and cycling stability (**Fig. 7b,c**).¹¹⁹

An environmentally friendly LIB using LFP cathode and transition metal oxide anode was proposed for high-power application¹²⁰: the battery was based on carbon-coated ZnFe_2O_4 nanoparticle anode and LiFePO_4 -multiwalled carbon nanotube cathode, both prepared by aqueous procedure with Na-carboxymethyl cellulose. The use of water and cellulose instead of organic toxic solvents and fluorine-containing PVDF is expected to significantly increase the sustainability of battery manufacturing process. The cell showed remarkable rate capability and delivered 50% of its theoretical capacity at 20C rate with respect to the cathode. Furthermore, it exhibited remarkable stability, retaining up to 85% of its initial capacity after more than 10000 cycles at about 10C with respect to the LiFePO_4 cathode (**Fig. 7d**). Pre-lithiation of the negative electrode allowed proper tuning of the cell potential (**Fig. 7e**), thus leading to high gravimetric energy and power density values of 202 Wh kg^{-1} and 3.72 W kg^{-1} , respectively.¹²⁰ Other works reported the combination of Me-oxide anodes and LFP cathodes with well suitable performances.^{64,121}

Lithium alloying anodes (Ge, Sn, Si) have shown particular suitability for LIBs in combination with LFP cathode. A Germanium (Ge) nanowires electrode improved through passivation by a dodecanethiol monolayer was proposed as suitable anode in LIB using LFP, with average discharge voltage of about 3.4 V and reversible capacity slightly lower than that obtained in the half-cell, however sufficient to light up a green light-emitting-diode (LED). The same cell in pouch-type configuration lighted up over 60 red LEDs, a white LED bulb, and powered an audio device.¹²² However, the use of hazardous chemicals in the anode synthetic recipe, such as benzene, toluene and hydrofluoric acid,¹²² might decrease the sustainability of a possible large-scale manufacturing process of this battery. A Further Ge/LFP LIB powering LED array employed germanium microcubes with a hierarchical structure supported on titanium foil.¹²³ The anode was prepared by heating GeO₂ microcubes deposited on the Ti foil at 550 °C under hydrogen atmosphere. The full cell tested at 0.1C rate showed flat charge plateau around 3.1 V and initial Coulombic efficiency of about 80%. After 100 cycles at 0.5C rate, the cell still kept a reversible capacity of 1123 mAh g⁻¹ with respect to the anode mass. A rate capability test revealed specific capacity at 0.1, 0.5, 1, and 2C rates (fixed lithiation rate of 0.2C) of 1150, 1109, 981, and 782 mAh g⁻¹ with respect to the anode mass, respectively.¹²³

A remarkable example of battery employing Li-alloy anode and LFP cathode within very safe and long-life configuration has been recently reported¹²⁴. The LIB was formed by a Sn-C nanocomposite anode, a LFP cathode, and a N-butyl-N-methylpyrrolidinium bis(fluoro-sulfonyl)imide (Py_{r14}FSI) lithium bis(trifluoromethanesulfonyl)imide (LiTFSI) IL-electrolyte, which allowed exceptional electrochemical performance in terms of reversible capacity, cycling stability, Coulombic efficiency and rate capability. The cell was expected to have low environmental impact, in view of the low cost and low toxicity of the electrode components, and high safety due to the use of non-volatile, poorly-flammable electrolyte, and structurally stable olivine and Li-alloying electrodes. The Sn-C/Py_{r14}FSI-LiTFSI/LFP LIB delivered a maximum capacity of 160 mA h g⁻¹ at an average working voltage of 3 V (**Fig. 7f**), good rate capability (**Fig. 7g**), and a Columbic efficiency

higher than 99.9% over more than 2000 charge/discharge cycles (**Fig. 7h**). The same work reported several ionic liquid electrolytes of different chemical structure, ionic conductivity, viscosity, electrochemical properties and lithium-interphase stability for LIBs application.¹²⁴ The efficient combined use of Li-alloy anodes and LFP cathodes was further demonstrated by several reports.^{125–}

131

Figure 7^{119,120,124}

The substitution of Fe within the olivine framework leads to higher working voltage of the cathode, thus enhancing the energy content of the full lithium-ion battery. However, only relatively few papers studied transition metal-substituted olivine materials in full cell configuration. A recent polymer LIB, formed by combining a $\text{LiMn}_{0.5}\text{Fe}_{0.5}\text{PO}_4$ olivine cathode, a nanostructured Sn–C anode, and a LiBOB-containing PVdF-based gel electrolyte, showed working voltage ranging from 2.8 to 3.6 V due to the $\text{Fe}^{3+}/\text{Fe}^{2+}$ and $\text{Mn}^{3+}/\text{Mn}^{2+}$ couples (**Fig. 8a**).¹³² The cell delivered a stable capacity of about 110 mAh g^{-1} with Coulombic efficiency of about 99% for 70 galvanostatic cycles (see **Fig. 8b**). Hence, the battery had an estimated theoretical energy density of about 360 Wh kg^{-1} with respect to the cathode, *i.e.*, a value expected to ensure a practical energy density comparable to commercial devices. The cell configuration has intrinsic high safety content as well as limited environmental issue due to the use of fluorine-free lithium salt, gelled electrolyte, alloy anode and olivine cathode characterized by a stable polyanionic framework.¹³² Furthermore, the $\text{LiMn}_{0.5}\text{Fe}_{0.5}\text{PO}_4$ material was prepared by an eco-friendly low-temperature solvothermal pathway in a water/ethylene glycol mixture, followed by annealing at 700 °C under Ar.

The substitution of Co for Fe leads to potential of 4.8 V vs. Li^+/Li due to the $\text{Co}^{3+}/\text{Co}^{2+}$ couple, thus enabling high-energy 5 V batteries.¹³³ However, the practical use of Co-based olivines is hindered by the environmental concerns due to the toxic and expensive cobalt.¹ Furthermore, LiCoPO_4 generally shows limited cycle life and reversible capacity lower than theoretical value. These shortcomings were partially mitigated by introducing Fe, Cr and Si within the LiCoPO_4 lattice. The cathode powders were prepared by solid-state treatment at 700 °C under nitrogen.¹³⁴ Neutron and

synchrotron diffraction data suggested higher Li-ion conductivity for the defect olivine structure of Cr,Si-LiCo_{0.9}Fe_{0.1}PO₄ with respect to LiCo_{0.9}Fe_{0.1}PO₄ and unsubstituted LiCoPO₄. The cathode was studied in a LIB in combination with graphite anode showing for the initial cycles at 1C rate a specific energy density as high as 550 Wh kg⁻¹, based on the cathode active mass, owing to the high operating voltage (**Fig. 8c**). This specific energy density value is higher than that one of the graphite/LiCoO₂ array. However, the energy density decreased to 510 Wh kg⁻¹ with respect to the cathode over 250 cycles (**Fig. 8d**).¹³⁴ Alternative and interesting examples of LIBs using mixed olivines and Li-conversion/alloying anodes are reported in a recent paper, combining LiFe_{0.25}Mn_{0.5}Co_{0.25}PO₄ olivine cathode, in which the Co-content was further decreased, either with Sn-Fe₂O₃-C or with Sn-C composites.¹³⁵ The cathode synthesis consisted of a low-temperature solvothermal treatment in water/ethylene glycol mixture and carbon coating at 700 °C under Ar. A similar heating procedure was used to the pyrolysis of Sn-containing resorcinol-formaldehyde gel to synthesize the Sn-C composite, while the Sn-Fe₂O₃-C material was prepared by simple mechanical high-energy milling of the bare powders, without any further thermal step. The resulting Sn-C/LiFe_{0.25}Mn_{0.5}Co_{0.25}PO₄ and Sn-Fe₂O₃-C/LiFe_{0.25}Mn_{0.5}Co_{0.25}PO₄ full cells were cycled at C/5 rate with respect to the cathode mass (1C = 170 mA g⁻¹) delivering a steady-state reversible capacity ranging from 90 to 100 mAh g_{cathode}⁻¹ at about 3.5 and 3.2 V. Taking into account a correction factor for inactive materials contributions of about 1/3, the estimated practical energy density of the Sn-C/LiFe_{0.25}Mn_{0.5}Co_{0.25}PO₄ and Sn-Fe₂O₃-C/LiFe_{0.25}Mn_{0.5}Co_{0.25}PO₄ cells were of about 120 and 100 Wh kg_{tot}⁻¹.

Figure 8^{132,134}

3. Lithium-ion batteries using spinel cathodes

LiMn₂O₄ (LMO) spinel-type oxide and its Ni-substituted version (*i.e.* 5 V-LNMO spinel) are Co-free cathode materials, characterized by relatively high operating voltage and rate capability, which may lead to high energy and remarkable power capability. These materials combine interesting electrochemical features such as low cost, environmental compatibility and high power density with respect to conventional layered oxides, while they generally suffer from capacity fade above 50 °C.²⁷

Spinel-type oxides were studied in full lithium-ion cells by several literature works reporting suitable performances.^{87,136–142} A highly efficient LIB using a commercial LMO cathode and a MnO_x-C nanocomposite anode, *i.e.*, low-cost and sustainable materials, has been reported (inset of **Fig. 9a**).¹⁴³ The anode, prepared by sol-gel route with pyrolysis at 850 °C in Ar, consisted of 5 to 30 nm-size MnO_x crystals (mainly MnO with Mn₃O₄ phase), embedded into a mesoporous carbon matrix (64 wt%). The full MnO_x-C/LMO cell was assembled in a charged state following a preconditioning procedure in order to avoid the first cycle irreversible capacity loss. The cell showed a voltage profile reflecting the overall electrochemical process between 2.0 and 4.1 V at 0.2C rate (**Fig. 9a**), as well as a capacity of about 100 mAh g⁻¹ with respect to the cathode. The cell capacity started to fade slowly from the 60th cycle, to give a 73% retention after 100 cycles. The initial capacity was almost completely recovered by lowering the C-rate to 0.1C (**Fig. 9b**), however with further slow fading and capacity retention of 60% upon 188 cycles. Proper electrode balancing by increasing the anode loading produced the optimal negative/positive electrode mass ratio and increased the MnO_x-C/LMO LIB stability up to 245 cycles at 2C rate (**Fig. 9c-d**).¹⁴³ A very interesting example of flexible, pouch-type LIB based on environmentally benign Mn employed spinel-structure LiMn₂O₄ cathode and conversion Mn₂O₃ anode, both within the nanowire configuration.¹⁴⁴ The same precursors, *i.e.*, MnOOH nanowires, formed from MnO₂ nanoflakes, were directly attached on Ti foils and subsequently transformed to Mn₂O₃ and LiMn₂O₄ by thermal annealing and reaction with lithium salt, respectively (scheme of **Fig. 9e**). The one-dimensional nanowire structures provided short lithium-ion diffusion path, good charge transport and volume flexibility for Li⁺ exchange, thus leading to good rate capability and cycling performance. The flexible Mn₂O₃/LiMn₂O₄ LIB delivered output voltage above 3 V, a specific capacity of 99 mAh g⁻¹ based on the cathode mass and had low thickness of 0.3 mm (see **Fig. 9f**). After 40 galvanostatic cycles, the capacity was of about 80 mAh g⁻¹.¹⁴⁴ A LIB of interest belonging to the same class was formed by coupling bare LiMn₂O₄ spinel cathode and carbon-coated Li₃Nd₃W₂O₁₂ (C-Li₃Nd₃W₂O₁₂) insertion anode, which has voltage as low as 0.3 V *vs.* Li⁺/Li.¹⁴⁵ The cell delivered at 1C rate a reversible capacity of 115 mAh g⁻¹ operating

within the 2.95 – 3.9 V voltage range, which leads to an energy density of about 390 Wh kg⁻¹. Furthermore, the cell showed improved cycling at the higher current rate, retaining about 71% and 93% of its initial reversible capacity after 100 cycles at 1C and 2 C rates, respectively. However, the use of neodymium-based electrode materials in commercial lithium-ion batteries might produce imbalance between demand and supply of neodymium,¹⁴⁶ thus likely hindering possible massive employment in scaled-up batteries.

Figure 9^{143,144}

LiNi_{0.5}Mn_{1.5}O₄ and metal substituted analogues represent very promising materials due to their high voltage and rate capability. This class of cathodes has been considered particularly suitable in terms of energy density for LIBs exploiting anodes of higher working voltage with respect to graphite, such as alloying, conversion and Ti-based electrodes.^{147–152} A very efficient LIB operating at 4.4 V coupled Sn-C nanostructured anode and high-rate Li[Ni_{0.45}Co_{0.1}Mn_{1.45}]O₄ spinel cathode prepared by sol-gel and coprecipitation approaches, respectively.¹⁵³ The battery delivered an estimated practical energy density of the order of 170 Wh kg⁻¹, exhibited extremely stable trend upon 100 cycles at 1C rate with respect to the cathode and demonstrated high rate capability by a retention of 85% of the initial capacity at 5C rate.¹⁵³ A LIB comprising a high-performance amorphous columnar silicon thin film anode prepared by DC magnetron sputtering and commercial LiNi_{0.5}Mn_{1.5}O₄ spinel cathode was proposed with fluoroethylene carbonate (FEC)-based electrolyte solution (FEC/DMC 1:4 with 1 M LiPF₆) with the aim of improving the cycle life.¹⁵⁴ The battery demonstrated hundreds of cycles, excellent charge–discharge efficiency and rate capability (**Fig. 10a-b**).¹⁵⁴ Another work¹⁵⁵ used a commercial spinel cathode with a carbon-coated Si-Cu₃Si-Al₂O₃ nanocomposite synthesized through a simple mechanochemical reaction. The incorporation of both the conductive Cu₃Si and electrochemically stable Al₂O₃ phases enhanced the cycling stability and rate capability, however with a decrease of specific capacity with increasing amount of Cu₃Si. The Si-Cu₃Si-Al₂O₃/LNMO battery cycled at 0.5C rate delivered reversible capacity of about 95 mAh g⁻¹

(based on the mass of the cathode material) at average working voltage above 3.5 V, a relatively good capacity retention of about 77.2% after 50 cycles with a high initial efficiency of about 86.3%. The enhanced electrochemical performance was attributed to the buffer Cu_3Si phase, which mitigated structural degradation and increased the anode conductivity.

Graphite¹⁵⁶ and graphene¹⁵⁷ anodes were also used in lithium-ion batteries employing LNMO cathode. Indeed, a graphite/LNMO LIB delivered a capacity of about 125 mAh g^{-1} at C/2 rate (30 °C), with capacity retention of 81% and a high Coulombic efficiency (over 99.6%) after 100 cycles.¹⁵⁸ The improvement of the LNMO electrochemical performance at high voltage in the above cell was achieved by addition to the electrolyte of an organo-phosphorus compound with an organic substituent, *i.e.*, tris(trimethylsilyl) phosphite (TMSP). TMSP mitigated the decomposition of LiPF_6 by hydrolysis, thus suppressing HF formation and avoiding Mn/Ni dissolution from the cathode; furthermore, TMSP formed a protective layer on the cathode surface.¹⁵⁸ Graphene and graphene oxide-based anodes have been widely explored in lithium half-cell, revealing remarkable performances. However, only few works demonstrated the suitability of this material as anodes in full lithium-ion cell, mostly due to the poor loading of graphene-based electrode, which leads to difficult N/P ratio setting during cell assembly. An attracting LIB has been recently obtained by coupling an exfoliated graphite/graphene nanosheets (EGNs) anode and a high-voltage LNMO spinel-structure cathode synthesized by wet chemistry route with calcination at 800 °C.¹⁵⁹ The binder-free anode, prepared by simple exfoliation of graphite in a solvent media and subsequent casting onto Cu support, showed a capacity exceeding by 40% that ascribed to commercial graphite in lithium half-cell, at very high C-rate, due to its particular structure and morphology, which allowed lithium intercalation into the graphite and insertion within the graphene nanosheets. The Li-ion battery operated at about 3.8 V, with a specific capacity of about 125 mAh g^{-1} , excellent efficiency and rate capability, as well as a cycle life up to 150 cycles. The estimated practical energy density of the above cell was of the order of 260 Wh kg^{-1} .¹⁵⁹

Very significant and efficient examples of LIBs based on LNMO cathodes were obtained by employing titanate anodes.^{57,160–168} The interest on titanate was justified by its electrochemical characteristics which match both capacity and rate capability of the LNMO cathode and facilitate the cell balance due to the flat voltage and relevant efficiency of the anode. Furthermore, LTO materials can be repeatedly cycled without inducing any electrolyte decomposition, since they operate at relatively high voltage values (about 1.5 V vs. Li⁺/Li), which fall within the electrochemical stability window of large part of the electrolytes. Therefore, the combination of LTO with high voltage spinel cathodes, operating at about 4.7 V vs. Li⁺/Li, leads generally to LIBs with working voltage of about 3.2 V. Accordingly, a spinel LNMO fiber cathode having on dimensional (1D) architecture was synthesized by electrospinning followed by high-temperature treatment, structurally and morphologically analyzed by various techniques, and coupled with an anatase TiO₂ fiber anode prepared with the same pathway. The full cell employed a gelled polyvinylidene fluoride-co-hexafluoropropylene (PVdF–HFP) electrolyte.¹⁶⁹ The TiO₂/LNMO cell delivered a reversible capacity of about 102 mAh g⁻¹ at 0.1C rate (1C = 150 mA g⁻¹) with an operating voltage centered at 2.8 V, excellent rate capability and stable cycling profiles with retention of about 86% over 400 cycles. Efficient LTO/LNMO LIBs were also reported with LiTFSI-pyrrolidinium bis(trifluoromethane-sulfonyl)imide ionic liquid electrolyte.¹⁷⁰ The LIBs revealed improvements in terms of capacity retention and Coulombic efficiency with respect to a benchmark cell using conventional carbonate-based electrolyte. Scanning electron microscopy (SEM) images and X-ray diffraction (XRD) patterns have shown maintained pristine morphology and structure of LNMO particles after 50 cycles at 0.5C. An extremely efficient and stable LIB advantageously combined a LTO negative electrode with a modified, Co-doped Li[Ni_{0.45}Co_{0.1}Mn_{1.45}]O₄ spinel-type cathode.¹⁷¹ The LTO/Li[Ni_{0.45}Co_{0.1}Mn_{1.45}]O₄ battery operated following the expected, very flat voltage profile centered at 3 V with extremely limited hysteresis between charge and discharge, which indicates high reversibility and fast kinetics (**Fig. 10c**). The battery delivered 128 mA h g⁻¹ with respect to the cathode at 1C rate for 500 cycles, with only 15% capacity loss (**Fig. 10d**). Moreover, the LIB has

shown satisfactory performances and very stable capacity within temperature ranging from -20 to $+55$ °C (**Fig. 10d**).¹⁷¹

The high voltage delivered by the spinel-type cathodes enables the use of several anode materials characterized by penalties in terms of operating potential, such as the lithium conversion electrodes (*e.g.*, metal oxides). Indeed, a recent work demonstrated the possible efficient use of CuO–MCMB composite, synthesized by easy high-energy ball milling process of low-cost precursors, in a LIB using a LNMO cathode.¹⁷² Such a high-energy milling approach did not require any further thermal treatment. The battery exhibited an average working voltage of 3.8 V, and delivered a capacity of about 120 mAh g_{cathode}^{-1} for over 100 cycles at 1C rate (148 mA g^{-1}) with respect to the cathode (**Fig. 10e**). Furthermore, rate capability tests up to 5C revealed reversible operation with capacity above 100 mAh g_{cathode}^{-1} . The CuO–MCMB/LiNi_{0.5}Mn_{1.5}O₄ battery had a theoretical energy density of the order of 420 Wh kg^{-1} , which is a value not far from that provided by the common graphite/LiCoO₂ system. Additional bonuses of this battery with respect to conventional systems were the lower cost and the limited environmental issues of the electrode materials. Other examples of LIBs combining conversion-type (NiO–MCMB) and conversion/alloying (Sn–Fe₂O₃–MCMB) anodes with high voltage spinel cathodes (LNMO) have been reported by the same group, with estimated energy density content of about 120 Wh kg^{-1} (**Fig. 10f**).^{173,174} Moreover, the CuO–Fe₂O₃–MCMB/Li_{1.35}Ni_{0.48}Fe_{0.1}Mn_{1.72}O₄ configuration has recently demonstrated very promising performances.¹⁷⁵ A further LIB based on CuO nanorod array anode and a commercial LNMO material with hierarchical structure exhibited capacity retention of 84% over 100 cycles at 0.5C rate with respect to the anode, and capacity of about 240 mAh g^{-1} at a C-rate as high as 10C (both referred to the anode mass).¹⁷⁶ A recent report studied a LIB based on 1D active materials prepared by a scalable procedure, *i.e.*, conversion-type α -Fe₂O₃ anode and an over-lithiated Li_{1.33}Ni_{0.5}Mn_{1.5}O₄ cathode. The electrode materials were prepared by electrospinning of fiber precursors followed by calcination.¹⁷⁷ The cathode was electrochemically over-lithiated before cell assembly in order to overcome irreversible capacity loss (ICL) in α -Fe₂O₃. The α -Fe₂O₃/Li_{1.33}Ni_{0.5}Mn_{1.5}O₄ cell, which employed a

PVdF-HFP-based gel electrolyte, revealed average working voltage of about 3.3 V, and delivered an energy density of about 193 Wh kg⁻¹ holding about 88% of the initial reversible capacity after 60 cycles when cycled at 100 mA g⁻¹ (referred to the anode mass). The energy density was calculated by multiplying the discharge capacity that takes into account the total mass of both active materials (about 59.02 mAh g⁻¹) and the working voltage. Further works reported on the use of LNMO-based cathodes in full cell configurations, combined with conversion-type,^{178–180} NASICON-type phosphate,¹⁸¹ VS₄,¹⁸² and vanadate anodes.⁶⁴

Figure 10^{154,171,172,174}

4. Next future lithium-ion batteries: sulfur and oxygen cathodes

Lithium-sulfur and lithium-oxygen batteries are certainly among the most attractive energy storage systems due to their extremely high energy content with respect to the conventional ones. Furthermore, they may actually decrease the lithium-ion battery issues in terms of cost and environmental concerns, due to the use positive electrodes based on cheap and sustainable materials, *i.e.*, carbon, oxygen and sulfur, instead of expensive and toxic Co-based oxides. Nevertheless, Li/S and Li/O₂ cells suffer from a safety issue due to the use of lithium metal at the anode side. A possible solution to this problem, allowing large scale diffusion of these appealing systems, is the replacement of the metal anode by a lithium-ion one.

Lithium-sulfur batteries have been widely investigated as alternative systems to the currently used LIBs, especially for the low cost and environmental impact of sulfur-based cathodes. However, commercialization of lithium-sulfur batteries has so far been limited due to problems associated with both the sulfur cathode and the lithium metal anode. These issues have been mitigated by using sulfur-based cathodes in combination with high-capacity composite anodes.^{183–193} A first lithium-ion sulfur battery combined a Sn-C anode, a Li₂S/C cathode prepared by low-energy ball milling under Ar atmosphere of Li₂S and carbon in 1:1 weight ratio, and a gel polymer electrolyte. The battery was characterized by theoretical specific energy and energy density of 2500 Wh kg⁻¹ and 2800 Wh l⁻¹,

respectively, *i.e.*, much greater values compared to those of any conventional lithium battery.¹⁹⁴ Further Li metal-free batteries combined S-based cathodes with Si alloy anodes.^{195–197} Thus, a lithium-ion battery using a Li₂S/mesoporous carbon composite cathode and Si nanowire anode delivered theoretical specific energy of 1550 Wh kg⁻¹ and discharge specific energy of 630 Wh kg⁻¹ based on the mass of the active electrode materials.¹⁹⁵ Another LIB based on S-cathode and silicon–carbon nanotube anode operated for over 1000 cycles delivering a specific capacity of 1470 mAh g_{sulfur}⁻¹ (720 mAh g_{cathode}⁻¹) with Coulombic efficiency approaching 99%.¹⁹⁶ An interesting example of polymer LIB based on sulfur-carbon cathode and Li-Sn-C nanostructured anode employed a PEO-polysulfide-added electrolyte.¹⁹⁷ The cell delivered stable capacity ranging from 500 to 1500 mAh g_{sulfur}⁻¹, depending on the cycling rate. The use of a polymer electrolyte and the replacement of the lithium metal with a Li-Sn-C nanostructured alloy improved the safety content of the battery. A Si/S LIB using lithiated Nafion-coated porous Si as anode and sulfur as cathode delivered specific capacity of 330 mAh g⁻¹ and energy density of 590 Wh kg⁻¹ based on the total mass of sulfur and silicon upon 100 cycles.¹⁹⁸

Recently, a highly reliable lithium-ion-sulfur battery, showing cycle performance comparable to that of lithium-ion batteries has been reported.¹⁹⁹ The LIB employed highly reversible, dual-type activated carbon (AC)-sulfur cathode (solid sulfur electrode and polysulfide catholyte) and a lithiated Si-SiO_x nanosphere anode. The cathode was easily prepared by melting elemental sulfur with activated carbon in 1:1 weight ratio at 135 °C. Afterwards, the resulting mixture was casted onto a gas diffusion layer (GDL). The Si-SiO_x/AC-S full cell showed remarkable battery performances in terms of high specific capacity, excellent charge–discharge efficiency, and remarkable cycle life. The cell delivered a specific capacity of 1100 mAh g_{sulfur}⁻¹ at 0.1C rate (1C = 1675 mAh g_{sulfur}⁻¹) with an average voltage of about 1.8 V, and a capacity of 750 mAh g_{sulfur}⁻¹ at 1C rate retained by 86% over 500 cycles, with an efficiency exceeding 98% (**Fig. 11a,b**).¹⁹⁹ Furthermore, B,N-Co-doped graphene supported sulfur (S@BNG) composite electrode was used in a lithium-ion-sulfur battery in combination with high performance lithiated Ge anode.²⁰⁰ The BNG with enriched pyridinic-N and

N–B/N=B bond as conductive host for sulfur electrode (having S loading of 75%) revealed strong interactions with polysulfide, which efficiently trapped the active sulfur within the electrode. The full Ge/S@BNG battery exhibited capacity of 530 mAh g⁻¹ with respect to the cathode (150 mAh g⁻¹ based on both cathode and anode) over 500 cycles at the rate of 1C. Therefore, it delivered a high reversible power density of 350 Wh kg⁻¹ (based on the mass of both cathode and anode) upon 100 cycles.

Few studies reported on metal-free, lithium-ion cells exploiting the Li/oxygen electrochemical process. A preliminary example evidencing the feasibility of this intriguing LIBs employed lithiated, nanostructured silicon-carbon composite at the anode side and oxygen supported by a gas diffusion layer, coated by Super-P carbon, at the cathode side (**Fig. 11c**).²⁰¹ The results of the study, based on X-ray diffraction and galvanostatic charge–discharge analyses, demonstrated the reversibility of the electrochemical process of the battery. The Li_xSi-C/C,O₂ cell exhibited a discharge voltage plateau centered at 2.40 V and was cycled by limiting both charge and discharge capacity at 1000 mAh g_{carbon}⁻¹ (**Fig. 11d**). Hence, the theoretical energy density of the complete (anode and cathode) Li_xSi-C/C,O₂ battery was estimated as 980 Wh kg⁻¹, which is remarkably higher value than that one offered by conventional lithium-ion batteries. However, the cell showed a continuous voltage decay upon cycling (**Fig. 11d**), which was likely attributed to oxygen attack on the Li_xSi-C anode by permeation across the electrolyte. Therefore, further work aimed at optimizing this cell design is required in order to solve this challenging issue. Obviously, the replacement of lithium metal with a lithium metal alloy entails a penalty in terms of both voltage and capacity; however, as for lithium-ion batteries, this drawback is favorably counterbalanced by the enhancement in safety. Therefore, the combined use of a lithium-ion anode with O₂ needs further work aimed at addressing unsolved issues limiting the cycle life.^{202–204}

Figure 11^{199,201}

5. Toward high-performance sustainable batteries

In the previous sections we focused the attention on the advances of the LIBs R&D towards the design of new and environmentally sustainable energy storage technologies, with particular emphasis on the strategies explored to improve the cycling performances. Several remarkable examples of LIBs of practical interest, employing layered, olivine, and spinel compounds as well as sulfur and oxygen-based cathodes, have been critically analyzed in terms of working voltage, cycling stability and Coulombic efficiency, with particular care on the main characteristics of the adopted cell configuration. Chemical, electrochemical and technological strategies attempted in order to overcome the benchmarks of currently available batteries have been explored through an overview of advanced LIBs using high-performance materials. Thus, the analysis of the various full cell configurations here reported highlights the prominent role of renewed battery chemistries at the anode, cathode and electrolyte sides, attempted by numerous research groups over the last few years, in determining remarkable progress of the LIB concept. Such an improvement nowadays meets the energy and power density requirements of a raising number of applications, ranging from advanced portable and mobile electronics to hybrid and full electric vehicles as well as large-size stationary storage. Beside novel active material formulations, the optimization of electrode morphology and architecture (including the use of nano-structures, composites or concentration-gradient materials) proved to be a suitable strategy to address the electrochemical cycling issues affecting various cathodes and anodes. This approach mainly aims to further enhance the electrochemical performances of alternative battery prototypes, to date only demonstrated as proof of concept, in order to favour their near-future transition from the laboratory to the production scale. The LIBs studies taken into account in the above reported sections outline the importance of critically selecting optimal cathode/anode weight ratio and voltage limits in order to achieve stable cycling performances and hold the full cell mass balance throughout the entire lifespan. Moreover, anode pre-lithiation procedures before full cell assembly proved to ensure high efficiency and cell balance for prolonged cycling, thus allowing the use of materials affected by huge first-cycle irreversibility, such as alloying and conversion anodes.

Combination of high performance and sustainability is becoming crucial for the development of new battery materials. Current research is making great efforts for optimizing new “green” electrodes and electrolytes able to ensure comparable or even higher performances than the conventional ones. In this respect, the replacement of oxide cathodes based on toxic and expensive metals, such as Co, with more sustainable active materials, containing Fe, Mn, and Al, may actually decrease the environmental issues of the battery. NMC and NCA electrodes, already on the market, represent a good compromise between satisfactory performances, reasonable safety and reduced environmental hazards. Following this trend, few papers have recently demonstrated the use in full cells of Li-rich layered materials, which further enhances the electrochemical features of the battery.

Furthermore, $\text{LiMn}_y\text{Fe}_x\text{PO}_4$ olivines are interesting eco-friendly compounds, characterized by suitable electrochemical behavior, low-cost and remarkable chemical stability, which may drastically improve the battery safety, particularly if polymer- and/or IL-based electrolytes are used. Several $\text{LiMn}_y\text{Fe}_x\text{PO}_4$ materials have been carefully optimized for application as high-performance positive electrodes in lithium half-cells,^{205,206} however only a few reports demonstrated their possible use in full lithium-ion cells. Moreover, the low density of olivine materials may represent an issue affecting the volumetric energy density of the full cell, especially in view of possible automotive applications.²⁰⁷ $\text{LiNi}_{0.5}\text{Mn}_{1.5}\text{O}_4$ spinel cathodes are very promising materials, since they combine high voltage, suitable electrochemical performance, even at high current rates, with limited environmental issues as compared to layered cathodes. Many literature papers have recently reported a vast array of lithium-ion cells employing LNMO materials that showed satisfactory behavior. As for the electrolyte solution, the use of fluorine-free salts, such as LiBOB, attracted large attention due to their environmental compatibility, despite the decreased ionic conductivity of the resulting solutions which may affect the power capability of the cell.

The exploitation of low-temperature synthesis methodologies, including solvothermal and mechanical milling approaches, might improve the sustainability of the cell. However, it is worth mentioning that solvothermal methods, mostly employed for the synthesis of phospho-olivine/carbon

and titanate/carbon composites, often require the use of organic co-solvents in addition to water, thus involving undesired byproducts in the synthesis pathway. The hydro/solvothermal step is generally carried out at temperature below 250 °C, however an additional high-temperature annealing in inert atmosphere is usually needed to improve the electronic conductivity of the material.

An interesting approach to make “green” batteries is the use of aqueous electrode processing, generally involving cellulose-based electrode binders. Following this trend, eco-friendly polymers may be also employed in substitution of conventional separators.

Finally, further remarkable breakthrough in battery sustainability may be achieved through the development of the lithium-sulfur and lithium-oxygen storage systems, holding the potential to allow a deep change of the LIB concept in the upcoming years. The encouraging results already achieved for lithium-sulfur batteries suggest a rapid growth of this technology in the close future, while several issues to be addressed still limit the lithium-oxygen systems. These new approaches might provide real advance towards the development of new and environmentally sustainable systems able to de-couple the global energy needs from the consumption of fossil fuels.

References

- 1 D. Larcher and J.-M. Tarascon, *Nat. Chem.*, 2014, **7**, 19–29.
- 2 P. Poizot and F. Dolhem, *Energy Environ. Sci.*, 2011, **4**, 2003.
- 3 J. B. Goodenough, *Energy Environ. Sci.*, 2014, **7**, 14–18.
- 4 A. Fotouhi, D. J. Auger, K. Propp, S. Longo and M. Wild, *Renew. Sustain. Energy Rev.*, 2016, **56**, 1008–1021.
- 5 L. Lu, X. Han, J. Li, J. Hua and M. Ouyang, *J. Power Sources*, 2013, **226**, 272–288.
- 6 F. Schipper, E. M. Erickson, C. Erk, J.-Y. Shin, F. F. Chesneau and D. Aurbach, *J. Electrochem. Soc.*, 2017, **164**, A6220–A6228.
- 7 A. Yoshino, in *Lithium-Ion Batteries*, ed. G. Pistoia, Elsevier, 2014, pp. 1–20.
- 8 L. Croguennec and M. R. Palacin, *J. Am. Chem. Soc.*, 2015, 150213175546000.

- 9 B. Scrosati, J. Hassoun and Y.-K. Sun, *Energy Environ. Sci.*, 2011, **4**, 3287.
- 10 M. Armand and J.-M. Tarascon, *Nature*, 2008, **451**, 652–657.
- 11 J. W. Choi and D. Aurbach, *Nat. Rev. Mater.*, 2016, **1**, 1–16.
- 12 W. J. Zhang, *J. Power Sources*, 2011, **196**, 13–24.
- 13 C.-M. Park, J.-H. Kim, H. Kim and H.-J. Sohn, *Chem. Soc. Rev.*, 2010, **39**, 3115–3141.
- 14 S. Goriparti, E. Miele, F. De Angelis, E. Di Fabrizio, R. Proietti Zaccaria and C. Capiglia, *J. Power Sources*, 2014, **257**, 421–443.
- 15 V. Aravindan, Y.-S. Lee and S. Madhavi, *Adv. Energy Mater.*, 2015, **5**, 1402225.
- 16 Y. Nishi, in *Lithium-Ion Batteries*, ed. G. Pistoia, Elsevier, 2014, pp. 21–39.
- 17 J. Hassoun and B. Scrosati, *J. Electrochem. Soc.*, 2015, **162**, A2582–A2588.
- 18 N. Takami, H. Inagaki, T. Kishi, Y. Harada, Y. Fujita and K. Hoshina, *J. Electrochem. Soc.*, 2009, **156**, A128.
- 19 P. Rozier and J. M. Tarascon, *J. Electrochem. Soc.*, 2015, **162**, A2490–A2499.
- 20 J. S. Weaving, F. Coowar, D. A. Teagle, J. Cullen, V. Dass, P. Bindin, R. Green and W. J. Macklin, *J. Power Sources*, 2001, **97–98**, 733–735.
- 21 M. M. Thackeray, S.-H. Kang, C. S. Johnson, J. T. Vaughey, R. Benedek and S. a. Hackney, *J. Mater. Chem.*, 2007, **17**, 3112.
- 22 J. Wang and X. Sun, *Energy Environ. Sci.*, 2015, **8**, 1110–1138.
- 23 K. Zaghib, A. Guerfi, P. Hovington, A. Vijh, M. Trudeau, A. Mauger, J. B. Goodenough and C. M. Julien, *J. Power Sources*, 2013, **232**, 357–369.
- 24 V. Aravindan, J. Gnanaraj, Y.-S. Lee and S. Madhavi, *J. Mater. Chem. A*, 2013, **1**, 3518–3539.
- 25 K. Amine, H. Yasuda and M. Yamachi, *Electrochem. Solid-State Lett.*, 2000, **3**, 178–179.
- 26 F. Mao, W. Guo, J. Ma, C. Zhao, X. Qian, V. Battaglia, R. Wang, Y.-S. Hu, S. Dai, T.-K. Sham, X. Sun, K. Amine and A. Williams, *RSC Adv.*, 2015, **5**, 105248–105258.
- 27 D. Liu, W. Zhu, J. Trottier, C. Gagnon, F. Barray, A. Guerfi, A. Mauger, H. Groult, C. M.

- Julien, J. B. Goodenough and K. Zaghib, *RSC Adv.*, 2014, **4**, 154–167.
- 28 H. D. Yoo, E. Markevich, G. Salitra, D. Sharon and D. Aurbach, *Mater. Today*, 2014, **17**, 110–121.
- 29 X. Ji, K. T. Lee and L. F. Nazar, *Nat. Mater.*, 2009, **8**, 500–506.
- 30 J. Kalhoff, G. G. Eshetu, D. Bresser and S. Passerini, *ChemSusChem*, 2015, **8**, 2154–2175.
- 31 E. G. Shim, T. H. Nam, J. G. Kim, H. S. Kim and S. I. Moon, *J. Power Sources*, 2007, **172**, 901–907.
- 32 S. S. Zhang, *J. Power Sources*, 2006, **162**, 1379–1394.
- 33 M. Lu, H. Cheng and Y. Yang, *Electrochim. Acta*, 2008, **53**, 3539–3546.
- 34 J. C. Bachman, S. Muy, A. Grimaud, H.-H. Chang, N. Pour, S. F. Lux, O. Paschos, F. Maglia, S. Lupart, P. Lamp, L. Giordano and Y. Shao-Horn, *Chem. Rev.*, 2016, **116**, 140–162.
- 35 V. Aravindan, J. Gnanaraj, S. Madhavi and H. K. Liu, *Chem. - A Eur. J.*, 2011, **17**, 14326–14346.
- 36 J. Ordoñez, E. J. Gago and A. Girard, *Renew. Sustain. Energy Rev.*, 2016, **60**, 195–205.
- 37 J. Muldoon, C. B. Bucur and T. Gregory, *Chem. Rev.*, 2014, **114**, 11683–11720.
- 38 N. Yabuuchi, K. Kubota, M. Dahbi and S. Komaba, *Chem. Rev.*, 2014, **114**, 11636–11682.
- 39 J. Xie and Q. Zhang, *J. Mater. Chem. A*, 2016, **4**, 7091–7106.
- 40 S. Passerini and B. Scrosati, *ECS Interface*, 2016, **25**, 85–87.
- 41 D. P. Abraham, M. M. Furczon, S. H. Kang, D. W. Dees and A. N. Jansen, *J. Power Sources*, 2008, **180**, 612–620.
- 42 Y. S. Jung, A. S. Cavanagh, L. Gedvilas, N. E. Widjonarko, I. D. Scott, S. H. Lee, G. H. Kim, S. M. George and A. C. Dillon, *Adv. Energy Mater.*, 2012, **2**, 1022–1027.
- 43 K. Rana, S. D. Kim and J.-H. Ahn, *Nanoscale*, 2015, **7**, 7065–71.
- 44 J. Wang, Y. Mai, H. Luo, X. Yan and L. Zhang, *J. Power Sources*, 2016, **334**, 58–64.
- 45 X. Su, C. Lin, X. Wang, V. A. Maroni, Y. Ren, C. S. Johnson and W. Lu, *J. Power Sources*,

- 2016, **324**, 150–157.
- 46 L. Cui, Y. Yang, C. Hsu and Y. Cui, *Nano Lett.*, 2009, **9 No.9**, 1–5.
- 47 M. H. Park, M. G. Kim, J. Joo, K. Kim, J. Kim, S. Ahn, Y. Cui and J. Cho, *Nano Lett.*, 2009, **9**, 3844–3847.
- 48 M. H. Park, Y. Cho, K. Kim, J. Kim, M. Liu and J. Cho, *Angew. Chemie - Int. Ed.*, 2011, **50**, 9647–9650.
- 49 F. W. Yuan and H. Y. Tuan, *Chem. Mater.*, 2014, **26**, 2172–2179.
- 50 S. Choi, J. Kim, N. S. Choi, M. G. Kim and S. Park, *ACS Nano*, 2015, **9**, 2203–2212.
- 51 X. Li, Z. Yang, Y. Fu, L. Qiao, D. Li, H. Yue and D. He, *ACS Nano*, 2015, **9**, 1858–1867.
- 52 X. Li, J. Liang, Z. Hou, W. Zhang, Y. Wang, Y. Zhu and Y. Qian, *J. Power Sources*, 2015, **293**, 868–975.
- 53 R. Bernhard, A. Latini, S. Panero, B. Scrosati and J. Hassoun, *J. Power Sources*, 2013, **226**, 329–333.
- 54 Q. Cheng, Z. Song, T. Ma, B. B. Smith, R. Tang, H. Yu, H. Jiang and C. K. Chan, *Nano Lett.*, 2013, **13**, 4969–4974.
- 55 J. Liu, X. Sun, Y. Li, X. Wang, Y. Gao, K. Wu, N. Wu and B. Wu, *J. Power Sources*, 2014, **245**, 371–376.
- 56 J. Guo, W. Zuo, Y. Cai, S. Chen, S. Zhang and J. Liu, *J. Mater. Chem. A*, 2015, **3**, 4938–4944.
- 57 N. Plylahan, M. Letiche, M. K. Samy Barr, B. Ellis, S. Maria, T. N. T. Phan, E. Bloch, P. Knauth and T. Djenizian, *J. Power Sources*, 2015, **273**, 1182–1188.
- 58 B. Liu, J. Zhang, X. Wang, G. Chen, D. Chen, C. Zhou and G. Shen, *Nano Lett.*, 2012, **12**, 3005–3011.
- 59 W. Li, X. Wang, B. Liu, S. Luo, Z. Liu, X. Hou, Q. Xiang, D. Chen and G. Shen, *Chem. - A Eur. J.*, 2013, **19**, 8650–8656.
- 60 X. Hou, X. Wang, B. Liu, Q. Wang, T. Luo, D. Chen and G. Shen, *Nanoscale*, 2014, **6**, 8858.

- 61 D. T. Ngo, R. S. Kalubarme, H. T. T. Le, C.-J. C.-N. C.-J. C.-N. Park and C.-J. C.-N. C.-J. C.-N. Park, *Nanoscale*, 2015, **7**, 2552–2560.
- 62 B. Wang, G. Wang and H. Wang, *Electrochim. Acta*, 2015, **156**, 1–10.
- 63 W. Xie, L. Gu, F. Xia, B. Liu, X. Hou, Q. Wang, D. Liu and D. He, *J. Power Sources*, 2016, **327**, 21–28.
- 64 N. Ding, X. Feng, S. Liu, J. Xu, X. Fang, I. Lieberwirth and C. Chen, *Electrochem. commun.*, 2009, **11**, 538–541.
- 65 C. Kim, M. Ko, S. Yoo, S. Chae, S. Choi, E.-H. Lee, S. Ko, S.-Y. Lee, J. Cho and S. Park, *Nanoscale*, 2014, **6**, 10604–10.
- 66 J.-I. Lee, E.-H. Lee, J.-H. Park, S. Park and S.-Y. Lee, *Adv. Energy Mater.*, 2014, **4**, 1301542.
- 67 W. C. Buttermann and H. E. Hilliard, *Mineral Commodity Profiles: Antimony, U.S. Geological Survey*, 2005.
- 68 I. H. Son, J. Hwan Park, S. Kwon, S. Park, M. H. Rummeli, A. Bachmatiuk, H. J. Song, J. Ku, J. W. Choi, J.-M. Choi, S.-G. Doo and H. Chang, *Nat. Commun.*, 2015, **6**, 7393.
- 69 D. T. Ngo, H. T. T. Le, C. Kim, J.-Y. Lee, J. G. Fisher, I.-D. Kim and C.-J. Park, *Energy Environ. Sci.*, 2015, **8**, 3577–3588.
- 70 B. W. C. Buttermann and J. D. Jorgenson, *Mineral Commodity Profiles: Germanium, U.S. Geological Survey*, 2005.
- 71 A. M. Gaikwad, B. V. Khau, G. Davies, B. Hertzberg, D. A. Steingart and A. C. Arias, *Adv. Energy Mater.*, 2015, **5**, 1401389.
- 72 M. S. Balogun, M. Yu, Y. Huang, C. Li, P. Fang, Y. Liu, X. Lu and Y. Tong, *Nano Energy*, 2015, **11**, 348–355.
- 73 X. Zhang, Z. Hou, X. Li, J. Liang, Y. Zhu and Y. Qian, *Electrochim. Acta*, 2016, **213**, 416–422.
- 74 C. Wang, L. Wu, H. Wang, W. Zuo, Y. Li and J. Liu, *Adv. Funct. Mater.*, 2015, 3524–3533.

- 75 S. J. Kropschot, *Molybdenum—A key component of metal alloys*, U.S. Geological Survey, 2010.
- 76 H. Zheng, Q. Sun, G. Liu, X. Song and V. S. Battaglia, *J. Power Sources*, 2012, **207**, 134–140.
- 77 S. H. Lee, C. S. Yoon, K. Amine and Y. K. Sun, *J. Power Sources*, 2013, **234**, 201–207.
- 78 U. Ulissi, M. Agostini, S. Ito, Y. Aihara and J. Hassoun, *Solid State Ionics*, 2016, **296**, 13–17.
- 79 M. Evertz, F. Horsthemke, J. Kasnatscheew, M. B??rner, M. Winter and S. Nowak, *J. Power Sources*, 2016, **329**, 364–371.
- 80 Y. Qian, C. Schultz, P. Niehoff, T. Schwieters, S. Nowak, F. M. Schappacher and M. Winter, *J. Power Sources*, 2016, **332**, 60–71.
- 81 L. Ji, H. Zheng, A. Ismach, Z. Tan, S. Xun, E. Lin, V. Battaglia, V. Srinivasan and Y. Zhang, *Nano Energy*, 2012, **1**, 164–171.
- 82 G. A. Elia, J. Wang, D. Bresser, J. Li, B. Scrosati, S. Passerini and J. Hassoun, *ACS Appl. Mater. Interfaces*, 2014, **6**, 12956–12961.
- 83 A. Bordes, K. Eom and T. F. Fuller, *J. Power Sources*, 2014, **257**, 163–169.
- 84 K. Eom, T. Joshi, A. Bordes, I. Do and T. F. Fuller, *J. Power Sources*, 2014, **249**, 118–124.
- 85 M. Agostini, U. Ulissi, D. Di Lecce, Y. Ahiara, S. Ito and J. Hassoun, *Energy Technol.*, 2015, **3**, 632–637.
- 86 A. Moretti, G. T. Kim, D. Bresser, K. Renger, E. Paillard, R. Marassi, M. Winter and S. Passerini, *J. Power Sources*, 2013, **221**, 419–426.
- 87 N. Takami, H. Inagaki, Y. Tatebayashi, H. Saruwatari, K. Honda and S. Egusa, *J. Power Sources*, 2013, **244**, 469–475.
- 88 J. Hassoun, P. Reale, S. Panero and B. Scrosati, *Isr. J. Chem.*, 2008, **48**, 229–234.
- 89 H. J. Kim, S. Choi, S. J. Lee, M. W. Seo, J. G. Lee, E. Deniz, Y. J. Lee, E. K. Kim and J. W. Choi, *Nano Lett.*, 2016, **16**, 282–288.

- 90 H. Hwang, H. Kim and J. Cho, *Nano Lett.*, 2011, **11**, 4826–4830.
- 91 R. Eisler, *Nickel hazards to fish, wildlife, and invertebrates: a synoptic review, U.S. Geological Survey*, 1998, vol. 34.
- 92 J. Ming, W. J. Kwak, S. J. Youn, H. Ming, J. Hassoun and Y.-K. Sun, *Energy Technol.*, 2014, **2**, 778–785.
- 93 H. Ye, Y.-X. Yin, S.-F. Zhang and Y.-G. Guo, *J. Mater. Chem. A*, 2014, **2**, 13293.
- 94 G. A. Elia, U. Ulissi, F. Mueller, J. Reiter, N. Tsiouvaras, Y.-K. Sun, B. Scrosati, S. Passerini and J. Hassoun, *Chem. - A Eur. J.*, 2016, **22**, 6808–6814.
- 95 H.-J. Noh, Z. Chen, C. S. Yoon, J. Lu, K. Amine and Y.-K. Sun, *Chem. Mater.*, 2013, **25**, 2109–2115.
- 96 J.-Y. Liao, S.-M. Oh and A. Manthiram, *ACS Appl. Mater. Interfaces*, 2016, **8**, 24543–24549.
- 97 C. Chae, H. J. Noh, J. K. Lee, B. Scrosati and Y. K. Sun, *Adv. Funct. Mater.*, 2014, **24**, 3036–3042.
- 98 B. Song, W. Li, P. Yan, S. M. Oh, C. M. Wang and A. Manthiram, *J. Power Sources*, 2016, **325**, 620–629.
- 99 B. Li, J. Wang, Z. Cao, P. Zhang and J. Zhao, *J. Power Sources*, 2016, **325**, 84–90.
- 100 S. Yamamoto, H. Noguchi and W. Zhao, *J. Power Sources*, 2015, **278**, 76–86.
- 101 S. Leijonmarck, A. Cornell, G. Lindbergh and L. Wågberg, *J. Mater. Chem. A*, 2013, **1**, 4671.
- 102 M. Agostini, L. G. Rizzi, G. Cesareo, V. Russo and J. Hassoun, *Adv. Mater. Interfaces*, 2015, **2**, 1500085.
- 103 J. Hassoun, F. Bonaccorso, M. Agostini, M. Angelucci, M. G. Betti, R. Cingolani, M. Gemmi, C. Mariani, S. Panero, V. Pellegrini and B. Scrosati, *Nano Lett*, 2014, **14**, 4901–4906.
- 104 C. Fasciani, S. Panero, J. Hassoun and B. Scrosati, *J. Power Sources*, 2015, **294**, 180–186.

- 105 A. Gören, J. Mendes, H. M. Rodrigues, R. E. Sousa, J. Oliveira, L. Hilliou, C. M. Costa, M. M. Silva and S. Lanceros-Méndez, *J. Power Sources*, 2016, **334**, 65–77.
- 106 G. Wang, S. Fang, D. Luo, L. Yang and S. Hirano, *Electrochem. commun.*, 2016, **72**, 148–152.
- 107 Q. Shi, W. Liu, Q. Qu, T. Gao, Y. Wang, G. Liu, V. S. Battaglia and H. Zheng, *Carbon N. Y.*, 2017, **111**, 291–298.
- 108 L. Woodruff and G. Bedinger, *Titanium—Light, strong, and white*, U.S. Geological Survey, 2013.
- 109 P. Manikandan, P. Periasamy and R. Jagannathan, *J. Mater. Chem. A*, 2013, **1**, 15397.
- 110 X. Zhang, V. Aravindan, P. S. Kumar, H. Liu, J. Sundaramurthy, S. Ramakrishna and S. Madhavi, *Nanoscale*, 2013, **5**, 5973–80.
- 111 C.-C. Yang, H.-C. Hu, S. J. J. Lin and W.-C. Chien, *J. Power Sources*, 2014, **258**, 424–433.
- 112 *Toxicological Profile for Vanadium*, Agency for Toxic Substances and Disease Registry, Public Health Service, 2012.
- 113 C. Wang, S. Wang, Y. B. He, L. Tang, C. Han, C. Yang, M. Wagemaker, B. Li, Q. H. Yang, J. K. Kim and F. Kang, *Chem. Mater.*, 2015, **27**, 5647–5656.
- 114 L. Persi, F. Croce and B. Scrosati, *Electrochem. commun.*, 2002, **4**, 92–95.
- 115 D. Choi, D. Wang, V. V. Viswanathan, I. T. Bae, W. Wang, Z. Nie, J. G. Zhang, G. L. Graff, J. Liu, Z. Yang and T. Duong, *Electrochem. commun.*, 2010, **12**, 378–381.
- 116 M. Mancini, F. Nobili, R. Tossici, M. Wohlfahrt-Mehrens and R. Marassi, *J. Power Sources*, 2011, **196**, 9665–9671.
- 117 J. Hassoun, M. Pfanzelt, P. Kubiak, M. Wohlfahrt-Mehrens and B. Scrosati, *J. Power Sources*, 2012, **217**, 459–463.
- 118 T. Gao, Q. Qu, G. Zhu, Q. Shi, F. Qian, J. Shao and H. Zheng, *Carbon N. Y.*, 2016, **110**, 249–256.
- 119 P. Xiong, L. Peng, D. Chen, Y. Zhao, X. Wang and G. Yu, *Nano Energy*, 2015, **12**, 816–823.

- 120 A. Varzi, D. Bresser, J. Von Zamory, F. Müller and S. Passerini, *Adv. Energy Mater.*, 2014, **4**, 1400054–1400063.
- 121 J. Hassoun, F. Croce, I. Hong and B. Scrosati, *Electrochem. commun.*, 2011, **13**, 228–231.
- 122 F.-W. Yuan, H.-J. Yang and H.-Y. Tuan, *ACS Nano*, 2012, **6**, 9932–9942.
- 123 C. Zhang, Z. Lin, Z. Yang, D. Xiao, P. Hu, H. Xu, Y. Duan, S. Pang, L. Gu and G. Cui, *Chem. Mater.*, 2015, **27**, 2189–2194.
- 124 G. A. Elia, U. Ulissi, S. Jeong, S. Passerini and J. Hassoun, *Energy Environ. Sci.*, 2016, **9**, 3210–3220.
- 125 J. Hassoun, S. Panero, G. Mulas and B. Scrosati, *J. Power Sources*, 2007, **171**, 928–931.
- 126 J. Hassoun, G. Derrien, S. Panero and B. Scrosati, *Electrochim. Acta*, 2009, **54**, 4441–4444.
- 127 J. Hassoun, A. Fericola, M. A. Navarra, S. Panero and B. Scrosati, *J. Power Sources*, 2010, **195**, 574–579.
- 128 M. Yao, K. Okuno, T. Iwaki, T. Awazu and T. Sakai, *J. Power Sources*, 2010, **195**, 2077–2081.
- 129 J. Hassoun, M. Wachtler, M. Wohlfahrt-Mehrens and B. Scrosati, *J. Power Sources*, 2011, **196**, 349–354.
- 130 J. Hassoun, D. J. Lee, Y. K. Sun and B. Scrosati, *Solid State Ionics*, 2011, **202**, 36–39.
- 131 S. Brutti, J. Hassoun, B. Scrosati, C.-Y. Y. Lin, H. Wu and H.-W. W. Hsieh, *J. Power Sources*, 2012, **217**, 72–76.
- 132 D. Di Lecce, C. Fasciani, B. Scrosati and J. Hassoun, *ACS Appl. Mater. Interfaces*, 2015, **7**, 21198–207.
- 133 D. Di Lecce, S. Brutti, S. Panero and J. Hassoun, *Mater. Lett.*, 2015, **139**, 329–332.
- 134 J. L. Allen, J. L. Allen, T. Thompson, S. A. Delp, J. Wolfenstine and T. R. Jow, *J. Power Sources*, 2016, **327**, 229–234.
- 135 D. Di Lecce, R. Verrelli and J. Hassoun, *Electrochim. Acta*, 2016, **220**, 384–390.
- 136 V. Aravindan, N. Shubha, Y. L. Cheah, R. Prasanth, W. Chuiling, R. R. Prabhakar and S.

- Madhavi, *J. Mater. Chem. A*, 2013, **c**, 308–316.
- 137 V. Aravindan, J. Sundaramurthy, P. S. Kumar, N. Shubha, W. C. Ling, S. Ramakrishna and S. Madhavi, *Nanoscale*, 2013, **5**, 10636–45.
- 138 L. J. Xi, H. K. Wang, S. L. Yang, R. G. Ma, Z. G. Lu, C. W. Cao, K. L. Leung, J. Q. Deng, A. L. Rogach and C. Y. Chung, *J. Power Sources*, 2013, **242**, 222–229.
- 139 R. Hu, W. Sun, Y. Chen, M. Zeng and M. Zhu, *J. Mater. Chem. A*, 2014, 9118–9125.
- 140 S. Jayaraman, V. Aravindan, P. Suresh Kumar, C. L. Wong, S. Ramakrishna and S. Madhavi, *ACS Appl. Mater. Interfaces*, 2014, **6**, 8660–8666.
- 141 A. Chaturvedi, V. Aravindan, P. Hu, R. R. Prabhakar, L. H. Wong, C. Kloc and S. Madhavi, *Appl. Mater. Today*, 2016, **5**, 68–72.
- 142 X. Xin, X. Zhou, J. Wu, X. Yao, Z. Liu, M. Technology, C. Academy and S. Ningbo, 2012, 11035–11043.
- 143 C. Chae, H. Park, D. Kim, J. Kim, E.-S. Oh and J. K. Lee, *J. Power Sources*, 2013, **244**, 214–221.
- 144 Y. Wang, Y. Wang, D. Jia, Z. Peng, Y. Xia and G. Zheng, *Nano Lett*, 2014, **14**, 1080–1084.
- 145 R. Satish, V. Aravindan, W. C. Ling, J. B. Goodenough and S. Madhavi, *Adv. Energy Mater.*, 2014, **4**, 1301715.
- 146 T. G. Goonan, *Rare Earth Elements — End Use and Recyclability*, U.S. Geological Survey, 2011.
- 147 J. Hassoun, S. Panero, P. Reale and B. Scrosati, *Int. J. Electrochem. Sci.*, 2006, **1**, 110–121.
- 148 J. Hassoun, G. Mulas, S. Panero and B. Scrosati, *Electrochem. commun.*, 2007, **9**, 2075–2081.
- 149 J. Hassoun, P. Reale and S. Panero, *J. Power Sources*, 2007, **174**, 321–327.
- 150 F. Croce, M. L. Focarete, J. Hassoun, I. Meschini and B. Scrosati, *Energy Environ. Sci.*, 2011, **4**, 921.
- 151 G. A. Elia, S. Panero, A. Savoini, B. Scrosati and J. Hassoun, *Electrochim. Acta*, 2013, **90**,

690–694.

- 152 G. A. Elia, F. Nobili, R. Tossici, R. Marassi, A. Savoini, S. Panero and J. Hassoun, *J. Power Sources*, 2015, **275**, 227–233.
- 153 J. Hassoun, K.-S. Lee, Y.-K. Sun and B. Scrosati, *J. Am. Chem. Soc.*, 2011, **133**, 3139–3143.
- 154 K. Fridman, R. Sharabi, R. Elazari, G. Gershinsky, E. Markevich, G. Salitra, D. Aurbach, A. Garsuch and J. Lampert, *Electrochem. commun.*, 2013, **33**, 31–34.
- 155 S.-O. Kim and A. Manthiram, *J. Power Sources*, 2016, **332**, 222–229.
- 156 J. S. Park, X. Meng, J. W. Elam, S. Hao, C. Wolverton, C. Kim and J. Cabana, *Chem. Mater.*, 2014, **26**, 3128–3134.
- 157 O. Vargas, Á. Caballero, J. Morales, G. A. Elia, B. Scrosati and J. Hassoun, *Phys. Chem. Chem. Phys.*, 2013, **15**, 20444–6.
- 158 Y.-M. Song, J.-G. Han, S. Park, K. T. Lee and N.-S. Choi, *J. Mater. Chem. A*, 2014, **2**, 9506–9513.
- 159 M. Agostini, S. Brutti and J. Hassoun, *ACS Appl. Mater. Interfaces*, 2016, **8**, 10850–10857.
- 160 D. Dambournet, I. Belharouak, J. Ma and K. Amine, *J. Power Sources*, 2011, **196**, 2871–2874.
- 161 L. M. O, J. Han and J. B. Goodenough, *Chem. Mater.*, 2011, **23**, 3404–3407.
- 162 V. Aravindan, W. C. Ling and S. Madhavi, *ChemPhysChem*, 2012, **13**, 3263–3266.
- 163 P. Suresh Kumar, V. Aravindan, J. Sundaramurthy, V. Thavasi, S. G. Mhaisalkar, S. Ramakrishna and S. Madhavi, *RSC Adv.*, 2012, **2**, 7983.
- 164 W. K. Pang, N. Sharma, V. K. Peterson, J.-J. Shiu and S. Wu, *J. Power Sources*, 2014, **246**, 464–472.
- 165 N. Plylahan, M. Letiche, M. Kenza, S. Barr and T. Djenizian, *Electrochem. commun.*, 2014, **43**, 121–124.
- 166 J. H. Kim, N. P. W. Pieczonka, P. Lu, Z. Liu, R. Qiao, W. Yang, M. M. Tessema, Y. K. Sun and B. R. Powell, *Adv. Mater. Interfaces*, 2015, **2**, 1–13.

- 167 U. Ulissi, J. Zimmermann, S. Brutti and J. Hassoun, *Electrochim. Acta*, 2016, **201**, 158–164.
- 168 G. F. Ortiz, M. Cabello, M. C. López, J. L. Tirado, M. J. McDonald and Y. Yang, *J. Power Sources*, 2016, **303**, 194–202.
- 169 N. Arun, V. Aravindan, S. Jayaraman, N. Shubha, W. C. Ling, S. Ramakrishna and S. Madhavi, *Nanoscale*, 2014, 8926–8934.
- 170 X. Cao, X. He, J. Wang, H. Liu, S. Roeser, B. R. Rad, M. Evertz, B. Streipert, J. Li, R. Wagner, M. Winter and I. Cekic-Laskovic, *ACS Appl. Mater. Interfaces*, 2016, acsami.6b07687.
- 171 H.-G. Jung, M. W. Jang, J. Hassoun, Y.-K. Sun and B. Scrosati, *Nat. Commun.*, 2011, **2**, 516.
- 172 R. Verrelli, J. Hassoun, A. Farkas, T. Jacob and B. Scrosati, *J. Mater. Chem. A*, 2013, **1**, 15329.
- 173 R. Verrelli and J. Hassoun, *ChemElectroChem*, 2015, **2**, 988–994.
- 174 R. Verrelli and J. Hassoun, *J. Power Sources*, 2015, **299**, 611–616.
- 175 D. Di Lecce, R. Verrelli, D. Campanella, V. Marangon and J. Hassoun, *ChemSusChem*, 2017.
- 176 W. Zhang, G. Ma, H. Gu, Z. Yang and H. Cheng, *J. Power Sources*, 2015, **273**, 561–565.
- 177 V. Aravindan, N. Arun, N. Shubha, J. Sundaramurthy and S. Madhavi, *Electrochim. Acta*, 2016, **215**, 647–651.
- 178 R. Verrelli, R. Brescia, A. Scarpellini, L. Manna, B. Scrosati and J. Hassoun, *RSC Adv.*, 2014, **4**, 61855–61862.
- 179 D. Lv, M. L. Gordin, R. Yi, T. Xu, J. Song, Y. B. Jiang, D. Choi and D. Wang, *Adv. Funct. Mater.*, 2014, **24**, 1059–1066.
- 180 R. Verrelli, N. Laszczynski, S. Passerini and J. Hassoun, *Energy Technol.*, 2016, n/a-n/a.
- 181 V. Aravindan, W. Chuiling and S. Madhavi, *Rsc Adv.*, 2012, **2**, 7534–7539.
- 182 X. Xu, S. Jeong, C. S. Rout, P. Oh, M. Ko, H. Kim, M. G. Kim, R. Cao, H. S. Shin and J. Cho, *J. Mater. Chem. A*, 2014, **2**, 10847–10853.

- 183 J. Hassoun, Y. K. Sun and B. Scrosati, *J. Power Sources*, 2011, **196**, 343–348.
- 184 J. Hassoun, J. Kim, D.-J. Lee, H.-G. Jung, S.-M. Lee, Y.-K. Sun and B. Scrosati, *J. Power Sources*, 2012, **202**, 308–313.
- 185 R. Elazari, G. Salitra, G. Gershinshy, A. Garsuch, A. Panchenko and D. Aurbach, *Electrochem. commun.*, 2012, **14**, 21–24.
- 186 S. Zheng, Y. Chen, Y. Xu, F. Yi, Y. Zhu, Y. Liu and J. Yang, *ACS Nano*, 2013, **7**, 10995–11003.
- 187 M. Agostini, J. Hassoun, J. Liu, M. Jeong, H. Nara, T. Momma, T. Osaka, Y. K. Sun and B. Scrosati, *ACS Appl. Mater. Interfaces*, 2014, **6**, 10924–10928.
- 188 K. Zhang, L. Wang, Z. Hu, F. Cheng and J. Chen, *Sci. Rep.*, 2014, **4**, 6467.
- 189 N. Moreno, M. Agostini, A. Caballero, J. Morales and J. Hassoun, *Chem. Commun.*, 2015, **51**, 14540–14542.
- 190 S. Thieme, J. Brueckner, A. Meier, I. Bauer, K. Gruber, J. Kaspar, A. Helmer, H. Althues, M. Schmuck and S. Kaskel, *J. Mater. Chem. A*, 2015, **3**, 3808–3820.
- 191 L. Wang, Y. Wang and Y. Xia, *Energy Environ. Sci.*, 2015, **8**, 1551–1558.
- 192 C.-Y. Fan, S.-Y. Liu, H.-H. Li, H.-F. Wang, H.-C. Wang, X.-L. Wu, H.-Z. Sun and J.-P. Zhang, *ACS Appl. Mater. Interfaces*, 2016, acsami.6b10515.
- 193 E. H. Mohan, B. V Sarada, R. V. Ram, G. Salian, A. K. Haridas, B. V. A. Rao and T. N. Rao, *Electrochim. Acta*, 2016, **219**, 1–20.
- 194 J. Hassoun and B. Scrosati, *Angew. Chemie Int. Ed.*, 2010, **49**, 2371–2374.
- 195 Y. Yang, M. T. McDowell, A. Jackson, J. J. Cha, S. S. Hong and Y. Cui, *Nano Lett.*, 2010, **10**, 1486–1491.
- 196 J. Brückner, S. Thieme, F. Böttger-Hiller, I. Bauer, H. T. Grossmann, P. Strubel, H. Althues, S. Spange and S. Kaskel, *Adv. Funct. Mater.*, 2014, **24**, 1284–1289.
- 197 M. Agostini and J. Hassoun, *Sci. Rep.*, 2015, **5**, 7591.
- 198 C. Shen, M. Ge, A. Zhang, X. Fang, Y. Liu, J. Rong and C. Zhou, *Nano Energy*, 2016, **19**,

68–77.

- 199 S.-K. Lee, S.-M. Oh, E. Park, B. Scrosati, J. Hassoun, M.-S. Park, Y.-J. Kim, H. Kim, I. Belharouak and Y.-K. Sun, *Nano Lett.*, 2015, **15**, 2863–2868.
- 200 W. Cai, J. Zhou, G. Li, K. Zhang, X. Liu, C. Wang, H. Zhou, Y. Zhu and Y. Qian, *ACS Appl. Mater. Interfaces*, 2016, **8**, 27679–27687.
- 201 J. Hassoun, H. G. Jung, D. J. Lee, J. B. Park, K. Amine, Y. K. Sun and B. Scrosati, *Nano Lett.*, 2012, **12**, 5775–5779.
- 202 G. A. Elia, R. Bernhard and J. Hassoun, *RSC Adv.*, 2015, **5**, 21360–21365.
- 203 G. A. Elia, D. Bresser, J. Reiter, P. Oberhumer, Y.-K. Sun, B. Scrosati, S. Passerini and J. Hassoun, *ACS Appl. Mater. Interfaces*, 2015, **7**, 22638–22643.
- 204 W.-J. Kwak, H.-J. Shin, J. Reiter, N. Tsiouvaras, J. Hassoun, S. Passerini, B. Scrosati and Y.-K. Sun, *J. Mater. Chem. A*, 2016, **4**, 10467–10471.
- 205 Y. K. Sun, S. M. Oh, H. K. Park and B. Scrosati, *Adv. Mater.*, 2011, **23**, 5050–5054.
- 206 S.-M. Oh, S.-T. Myung, J. B. Park, B. Scrosati, K. Amine and Y.-K. Sun, *Angew. Chemie Int. Ed.*, 2012, **51**, 1853–6.
- 207 D. Andre, S. Kim, P. Lamp, F. Lux and F. Maglia, *J. Mater. Chem. A Mater. energy Sustain.*, 2015, **3**, 6709–6732.

List of Schemes

Scheme 1. Representation of the Review structure, summarizing the main topics surveyed.

List of Figures

Figure 1. Characteristics of a flexible LTO/LCO lithium-ion cell. (a) Schematic representation of the pouch-cell. (b) Areal capacity (mAh cm^{-2}) of the full cell cycled for 450 cycles at C/2 rate. The full cell had a total active area of $2.5 \times 2.5 \text{ cm}^2$ and LTO and LCO loading of 13.4 and 12.5 mg cm^{-2} , respectively. (c) Areal capacity (mAh cm^{-2}) and columbic efficiency (%) of the full cell cycled between C/4 and 1C rates. (d) Galvanostatic charge/discharge curves for the full cell cycled between C/4 to 1C rate. The capacity at C/4, C/2 and 1C rate was 117, 104 and 90 mAh g^{-1} , respectively. Columbic efficiency of all the batteries was above 99.5%. Electrolyte: 1 M solution of LiPF_6 in EC:DEC 1:1. Reproduced with permission.⁷¹ Copyright 2014 WILEY-VCH Verlag GmbH & Co. KGaA, Weinheim.

Figure 2. Characteristics of a $\text{TiO}_2\text{-MoO}_3/\text{LCO}$ lithium-ion cell. (a) Schematic illustration of structural features of the synergistic $\text{TiO}_2\text{-MoO}_3$ nanowire array. (b) SEM image of the optimized $\text{TiO}_2\text{-MoO}_3$ hybrid array (optical image in inset). (c) Schematic illustration of the full cell. (d) Stored charge of both the $\text{Li}/\text{TiO}_2\text{-MoO}_3$ half-cell and the $\text{TiO}_2\text{-MoO}_3/\text{LCO}$ full cell at different currents. (e) First three charge–discharge curves of the full cell. (d) Cycling performance and Coulombic efficiency of the full cell at 50 $\text{mA g}_{\text{total}}^{-1}$. Electrolyte: 1 M LiPF_6 in EC:DEC 1:1 v/v. Voltage limits: 1.0–4 V. Reproduced with permission.⁷⁴ Copyright 2015 WILEY-VCH Verlag GmbH & Co. KGaA, Weinheim.

Figure 3. Characteristics of a $\text{Sn-C}/\text{Pyr}_{14}\text{TFSI-LiTFSI}/\text{NMC}$ lithium-ion cell. (a-b) Galvanostatic cycling performances in terms of (a) voltage profiles and (b) cycling behavior of the full cell. (c) Evolution of the interface resistance of the full cell upon cycling. (d) Ex situ SEM images of the electrode materials (Sn-C and NMC) after cycling. Electrolyte: 0.2 mol kg^{-1} LiTFSI in $\text{Pyr}_{14}\text{TFSI}$.

Voltage limits: 2.5 – 4.0 V. Current rate: 25 mA g⁻¹. Temperature: 40°C. Reproduced with permission.⁹⁴ Copyright 2016 Wiley-VCH Verlag GmbH & Co. KGaA, Weinheim.

Figure 4. Lithium-ion batteries based on concentration gradient layered cathodes. **(a-d)** Characteristics of a MCMB/Li[Ni_{0.60}Co_{0.15}Mn_{0.25}]O₂ lithium-ion cell. **(a)** Cross-sectional SEM and EPMA mapping of Ni, Co, and Mn within a single lithiated Li[Ni_{0.60}Co_{0.15}Mn_{0.25}]O₂ cathode particle; **(b)** integrated atomic ratio of transition metals as a function of the distance from the center of the particle for the lithiated Li[Ni_{0.60}Co_{0.15}Mn_{0.25}]O₂ cathode. **(c-d)** Cycling performance in laminated-type Al-pouch cell in terms of **(c)** specific discharge capacity (mAh g⁻¹) and **(d)** discharge capacity (mAh). Electrolyte: 1.2 M LiPF₆ in EC:EMC 3:7 v/v. Current rate: 1 C (corresponding to 180 mA g⁻¹). Voltage limits: 3.0 – 4.4 V. Temperature: 25°C and 55°C. Reproduced with permission.⁹⁵ Copyright 2013 American Chemical Society. **(e-f)** Characteristics of a Si-C/Li[Ni_{0.75}Co_{0.1}Mn_{0.15}]O₂ lithium-ion cell. **(e)** Cycling performances of the Li[Ni_{0.75}Co_{0.1}Mn_{0.15}]O₂ cathode in lithium half-cells at C/3 rate. **Inset:** elemental intensity ratio of Mn/Ni across the cycled cathode particle based on the EDS line-scanning data and cross section SEM image. **(f)** Cycling performance of pouch-type full cell at C/3 rate (image in **inset**). Electrolyte: 1.2 M LiPF₆ in EC:EMC 3:7 v/v. Voltage limits: 2.5 – 4.4 V. Reproduced with permission.⁹⁶ Copyright 2016 American Chemical Society.

Figure 5. Characteristics of a graphite/xLi₂MnO₃·(1-x)LiNi_{0.7}Co_{0.15}Mn_{0.15}O₂ lithium-ion cell. SEM images and SEM-EDX line scan of Ni, Co, and Mn at cross section of xLi₂MnO₃·(1-x)LiNi_{0.7}Co_{0.15}Mn_{0.15}O₂ particles: **(a)** x = 0 and **(b)** x = 0.10. **(c)** Schematic representation of the phase composition of a xLi₂MnO₃·(1-x)LiNi_{0.7}Co_{0.15}Mn_{0.15}O₂ particle. **(d)** Laminated full pouch-cell cycled at C/10 rate for first 2 cycles and at C/3 rate for the rest of the cycles. Electrolyte: 1 M LiPF₆ in EC:DEC 1:1 v/v. Voltage limits: 2.5 – 4.4 V. Temperature: 25°C. Reproduced with permission.⁹⁸ Copyright 2016 Elsevier B.V.

Figure 6. Characteristics of a LTO/LFP lithium-ion cell. Photographs of LTO/LFP full cell **(a)** before and **(b)** after 8000 cycles at current density of 30C rate. **(c-d)** Rate capability in terms of **(c)** cycling

behavior and **(d)** voltage profiles of the LFP/LTO battery at various (dis)charge rates from 0.5C to 80C. **(e)** Cycling performance at a rate of 30C/30C (charge/discharge). Specific capacity referred to the LTO anode. Electrolyte: 1 M LiPF₆ in EC/DEC/EMC 1:1:1 v/v. Voltage limits: 1.0 – 2.3 V. Temperature: 25°C. Reproduced with permission.¹¹³ Copyright 2015 American Chemical Society.

Figure 7. (a-c) Characteristics of a 2D, all-nanosheet-based ZnMn₂O₄-graphene/LFP lithium-ion cell. **(a)** Schematic of the cell. **(b)** Cycling performances of the all-nanosheet-based full battery and a control full battery together; Coulombic efficiency of all-nanosheet-based full battery. Current rate: 0.2C. **(c)** Cycling performances of all-nanosheet-based full battery at 2C, 5C and 10C. Electrolyte: 1 M LiPF₆ in EC:DEC 1:1 v/v. Voltage limits: 0.9 – 3.9 V. Reproduced with permission.¹¹⁹ Copyright 2015 Elsevier Ltd. **(d-e)** Characteristics of a C-ZnFe₂O₄/LFP-multiwalled carbon nanotube (CNT) lithium-ion battery. **(d)** Long-term cycling stability applying a current density of 3 mA cm⁻² and Coulombic efficiency of ZFO/LFP-CNT full cells employing anodes with different degrees of lithiation. **(e)** Selected electrode and cell voltage profiles evolution upon cycling. Specific capacity values are referred to the active material amount of both the limiting cathode (*i.e.*, LFP) and the sum of the anode and cathode (*i.e.*, TOT = LFP+ZFO). Electrolyte: 1 M LiPF₆ in EC:DEC 3:7 v/v. Li reference electrode employed in the full-cells for monitoring the individual electrode potentials. Temperature: 20°C. Reproduced with permission.¹²⁰ Copyright 2014 WILEY-VCH Verlag GmbH & Co. KGaA, Weinheim. **(f-h)** Characteristics of a Sn-C/Pyr₁₄FSI-LiTFSI/LFP lithium-ion cell. **(f)** Selected steady-state voltage signatures and **(g)** cycling behavior with Coulombic efficiency of the full cell cycled at increasing currents, *i.e.*, 25, 50, 75, 100, 150, 200 and 250 mA g⁻¹ (0.12, 0.24, 0.36, 0.48, 0.72, 0.96, and 1.2 mA cm⁻², respectively). **(h)** Cycling behavior with Coulombic efficiency of the full cell in a long-term galvanostatic cycling test at 100 mA g⁻¹ (1.2 mA cm⁻²). Electrolyte: 0.2 mol kg⁻¹ LiTFSI in Pyr₁₄FSI. Voltage limits: 2.0 – 3.8 V. Temperature: 40°C. Specific capacity (mAh g⁻¹) and specific current (mA g⁻¹) are given with respect to the LFP cathode active mass. Reproduced with permission.¹²⁴ Copyright 2016 The Royal Society of Chemistry.

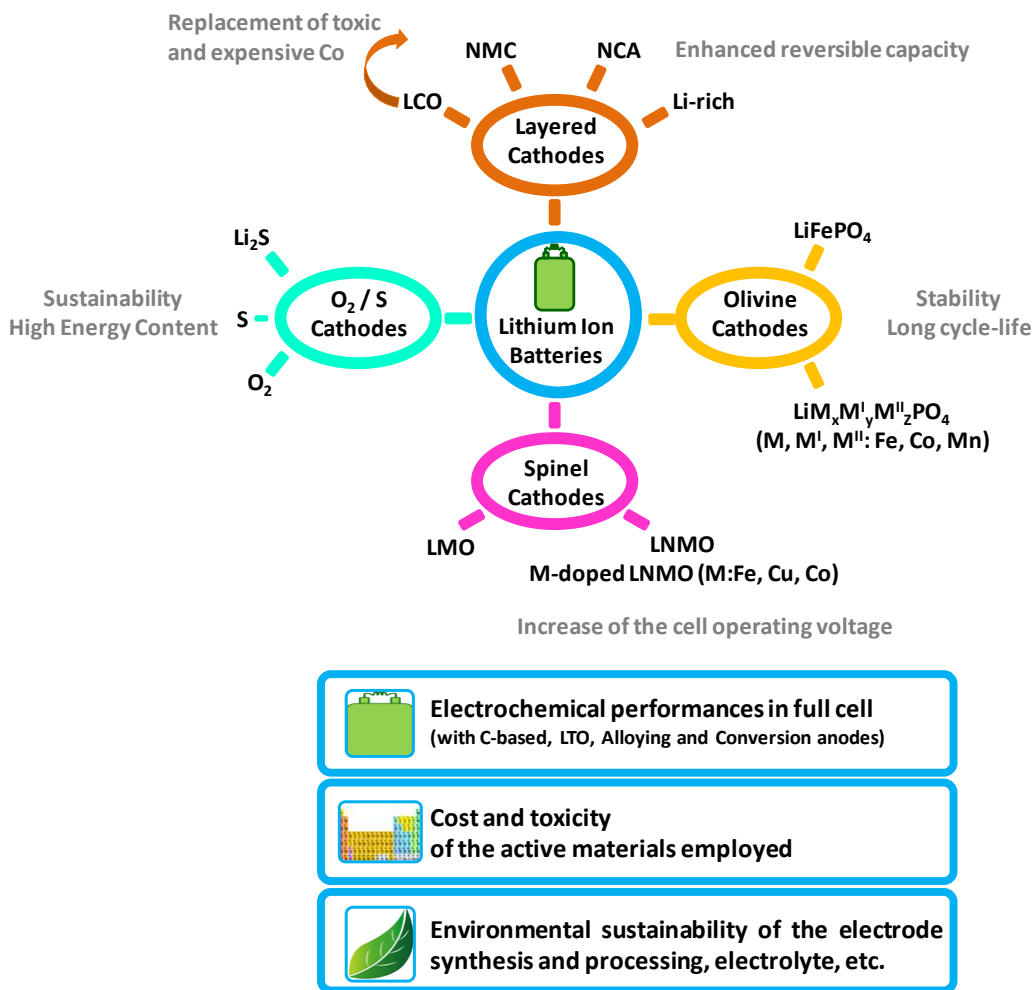
Figure 8. (a-b) Characteristics of a Sn-C/GPE/LiMn_{0.5}Fe_{0.5}PO₄ lithium-ion cell cycled at 0.2C rate with respect to the cathode (1C = 170 mA g_{cathode}⁻¹). **(a)** Galvanostatic response in terms of voltage profiles of the 1st, 5th, 10th, 15th, and 20th cycle of the Sn-C/GPE/LiMn_{0.5}Fe_{0.5}PO₄ full cell; **inset** of panel **a**: voltage profiles of the 1st, 2nd, and 4th cycle of the full-cell cycled at 40°C using. **(d)** Cycling behavior and corresponding Coulombic efficiency of the Sn-C/GPE/LiMn_{0.5}Fe_{0.5}PO₄ full cell. Electrolyte: gel polymer electrolyte (GPE) based on PVDF and 0.7 M LiBOB in 1:1:3 EC:PC:DMC w/w. Voltage limits: 1.6 – 4.2 V. Temperature: 25°C except for **inset** of panel **b**. Reproduced with permission.¹³² Copyright 2015 American Chemical Society. **(c-d)** Characteristics of a graphite/Cr,Si-LiCo_{0.9}Fe_{0.1}PO₄ lithium-ion cell in terms of **(e)** voltage profile of the 2nd (**solid blue line**) and 250th cycles (**dashed red line**) as well as **(f)** cycling behavior. Electrolyte: 1.2 M LiPF₆ in EC:EMC 3:7 w/w with 2 wt% tris(trimethylsilyl) phosphite. Cycling procedure: first cycle between 4.85 – 3.0 V at a constant C/20 current; subsequent cycles with charge at a C/2 constant current to 4.85 V, charge at a constant 4.85 V voltage until the current was less than C/15, and discharge at a 1C constant current to 3.5 V. Reproduced with permission.¹³⁴ Copyright 2016 Elsevier B.V.

Figure 9. (a-d) Characteristics of a MnO_x-C/LiMn₂O₄ lithium-ion cell. **(a)** Voltage profile and schematic cell representation in **inset**. **(b)** Cycling performance of a full cell with 4.5 and 1.2 mg cm⁻² loading for cathode and anode, respectively, cycled at 0.2C rate for 100 cycles and then at 0.1C rate for up to 188 cycles. **(c)** Cycling performance of a full cell with 3.7 and 1.8 mg cm⁻² loading for cathode and anode, respectively, cycled at 0.2C rate for up to 195 cycle, and **(d)** rate performance of the same cell. Electrolyte: 1 M LiPF₆ in EC:DMC 3:7 v/v. Voltage limits: 2.0 and 4.1 V. Current rates and capacity referred to the cathode mass (1C = 148 mA g_{cathode}⁻¹). Reproduced with permission.¹⁴³ Copyright 2013 Elsevier B.V. **(e-f)** Characteristics of a flexible Mn₂O₃/LiMn₂O₄ lithium-ion cell. **(e)** Schematic of the synthesis and fabrication of the full cell. **(f)** Cycling performance (**red curve**) and Coulombic efficiency (**black curve**) of the full cell. The cell is fully extended in the first 20 cycles and folded from the 21st to 40 cycles, as shown by optical images and the black arrows in the **insets**.

Electrolyte: 1 M LiPF₆ in EC:DEC:DMC 1:1:1 w/w. Voltage limits: 4.2 – 1.5 V. Reproduced with permission.¹⁴⁴ Copyright 2014 American Chemical Society.

Figure 10. (a-b) Characteristics of a Si/LNMO lithium-ion cell. Cell performances in terms of (a) voltage profiles and (b) cycling behavior. Electrolyte: 1 M LiPF₆ in FEC:DMC 1:4. Current rate: 0.5C (10 initial cycles at C/8 rate). Reproduced with permission.¹⁵⁴ Copyright 2013 Elsevier B.V. (c-d) Characteristics of a Li₄Ti₅O₁₂/Li[Ni_{0.45}Co_{0.1}Mn_{1.45}]O₄ lithium-ion cell. Cell performances at several temperatures (*i.e.*, from – 20 to + 55°C) in terms of (c) voltage profiles and (d) cycling behavior at 1C and 0.5C rates. Electrolyte: 1.2 M LiPF₆ in EC:DMC 3:7 v/v. Reproduced with permission.¹⁷¹ Copyright 2011 Macmillan Publishers Limited. (e) Characteristics of a CuO–MCMB/LNMO lithium-ion cell in terms of voltage profiles and (inset) cycling behavior at 1C rate with respect to the cathode (148 mA g_{cathode}⁻¹). Electrolyte: 1 M LiPF₆ in EC:DMC 1:1 w/w. Voltage range: 1.5 – 5.0 V. Room temperature. Reproduced with permission.¹⁷² Copyright The Royal Society of Chemistry 2013. (f) Characteristics of a Sn-Fe₂O₃-C/LNMO cell in terms of voltage profiles of the full cell (blue curve) and of its anodic and cathodic components (green and red curves, respectively), as well as (inset) full-cell cycling behavior. Electrolyte: 1 M LiPF₆ in EC:DMC 1:1 w/w. Current rate: C/3 with respect to the cathode (50 mA g_{cathode}⁻¹). Three-electrode configuration. Room temperature. Reproduced with permission.¹⁷⁴ Copyright 2015 Elsevier B.V.

Figure 11. (a-b) Characteristics of a Si-SiO_x/dual-type activated carbon-S lithium-ion cell. (a) cyclic behavior and (b) voltage profiles of the full cell cycled at 1C rate. Inset of panel a: Schematic representation of the cell. Electrolyte: 0.05 M Li₂S₈, 1 M LiTFSI, 0.4 M LiNO₃ in DME:DOL 1:1 v/v. Voltage limits: 2.8 – 0.8 V. 1C = 1675 mAh g⁻¹ versus overall sulfur weight. Temperature: 30°C. Reproduced with permission.¹⁹⁹ Copyright 2015 American Chemical Society. (c-d) Characteristics of a Li_xSi-C/C₂O₂ lithium-ion cell. (c) Schematic representation and (d) voltage profiles of the Li_xSi-C/C₂O₂ cell. Electrolyte: LiCF₃SO₃:TEGDME 1:4 mol/mol. Cycling current: 200 mA g_{carbon}⁻¹. Room temperature. Reproduced with permission.²⁰¹ Copyright 2012 American Chemical Society.



Scheme 1

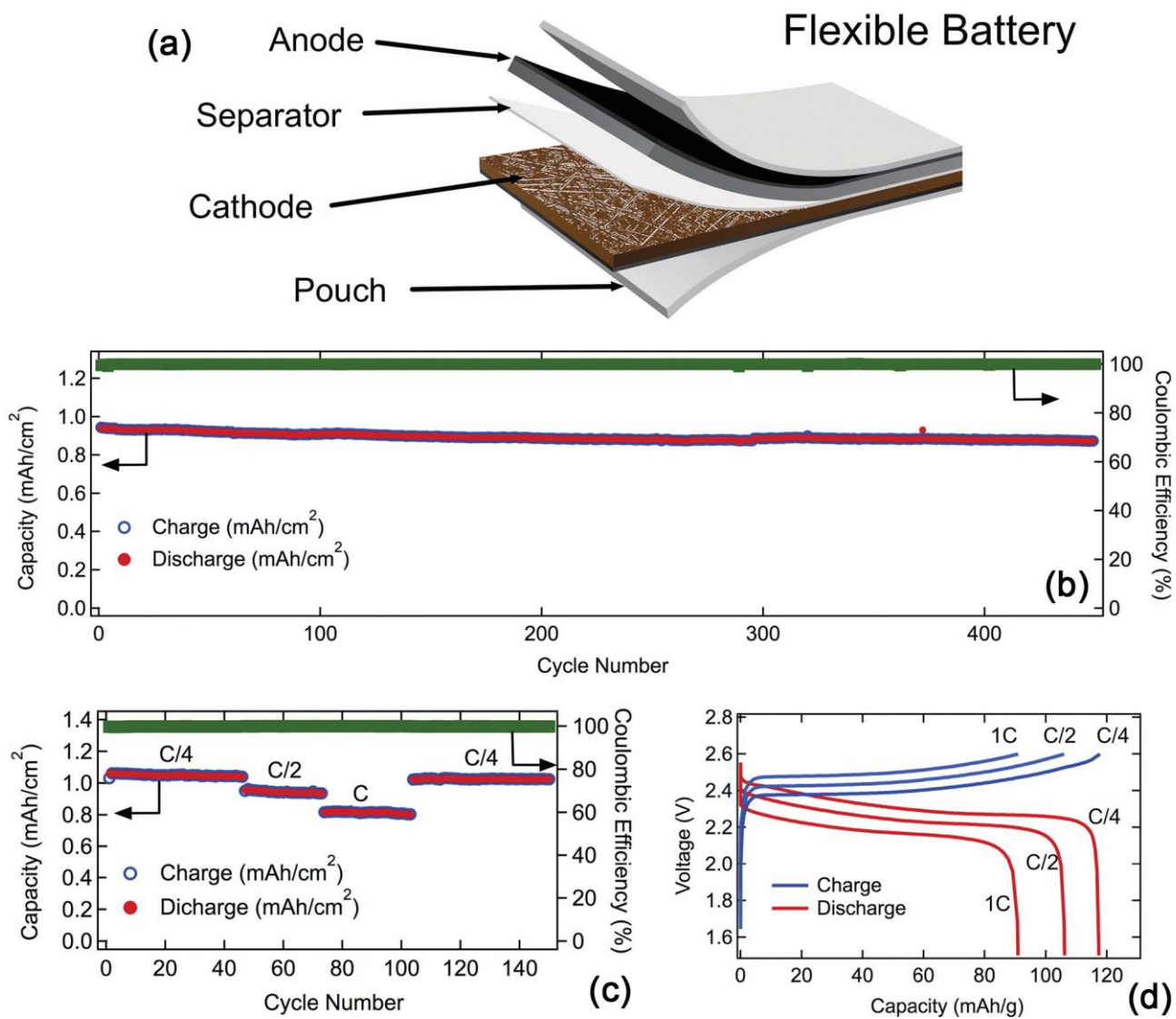


Figure 1

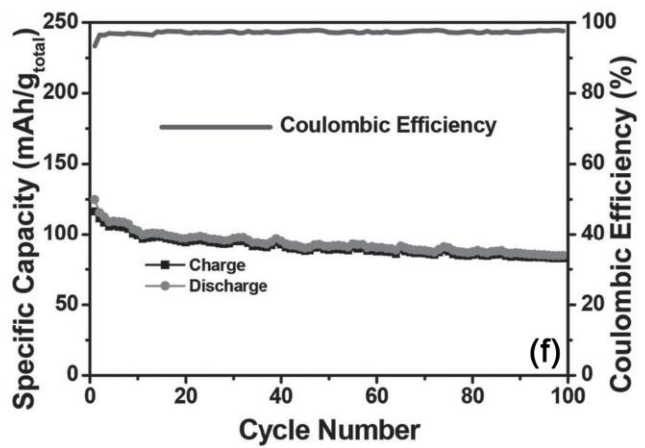
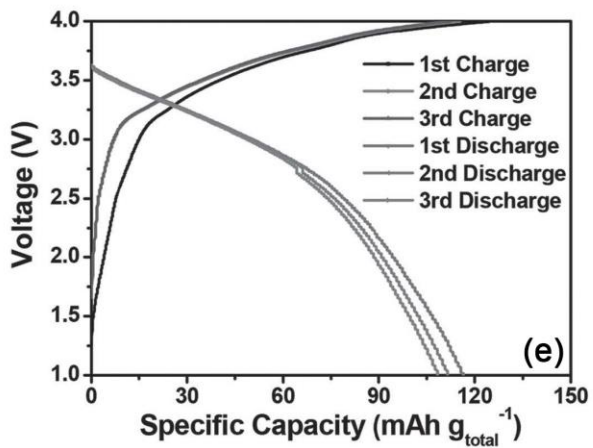
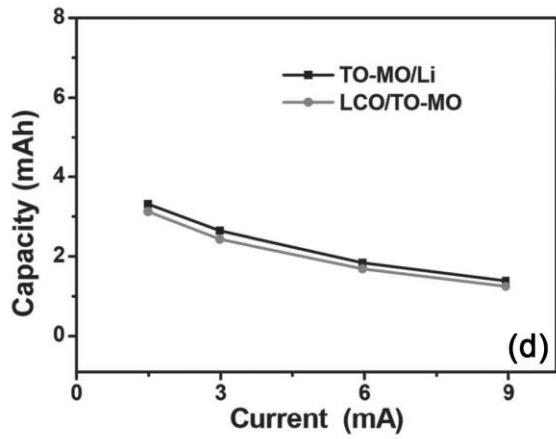
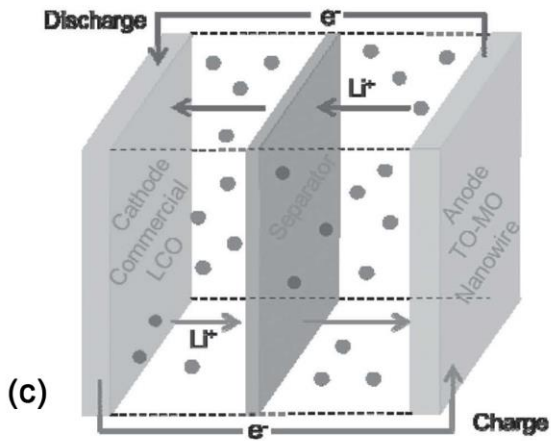
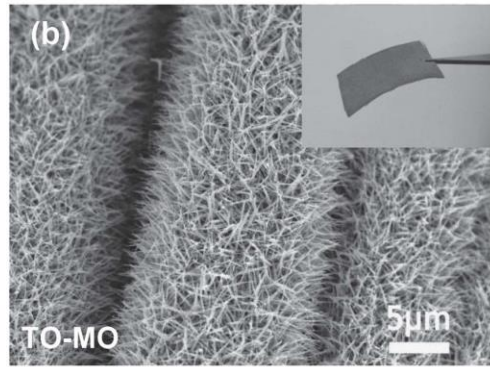
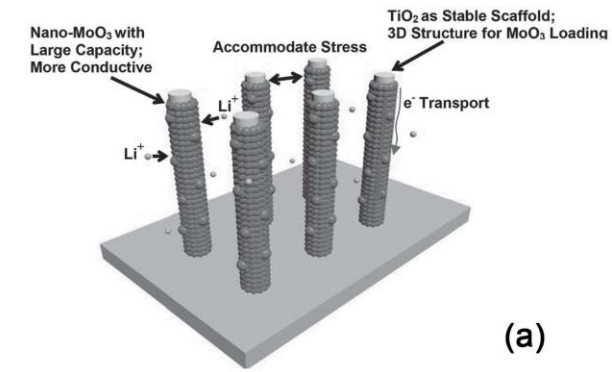


Figure 2

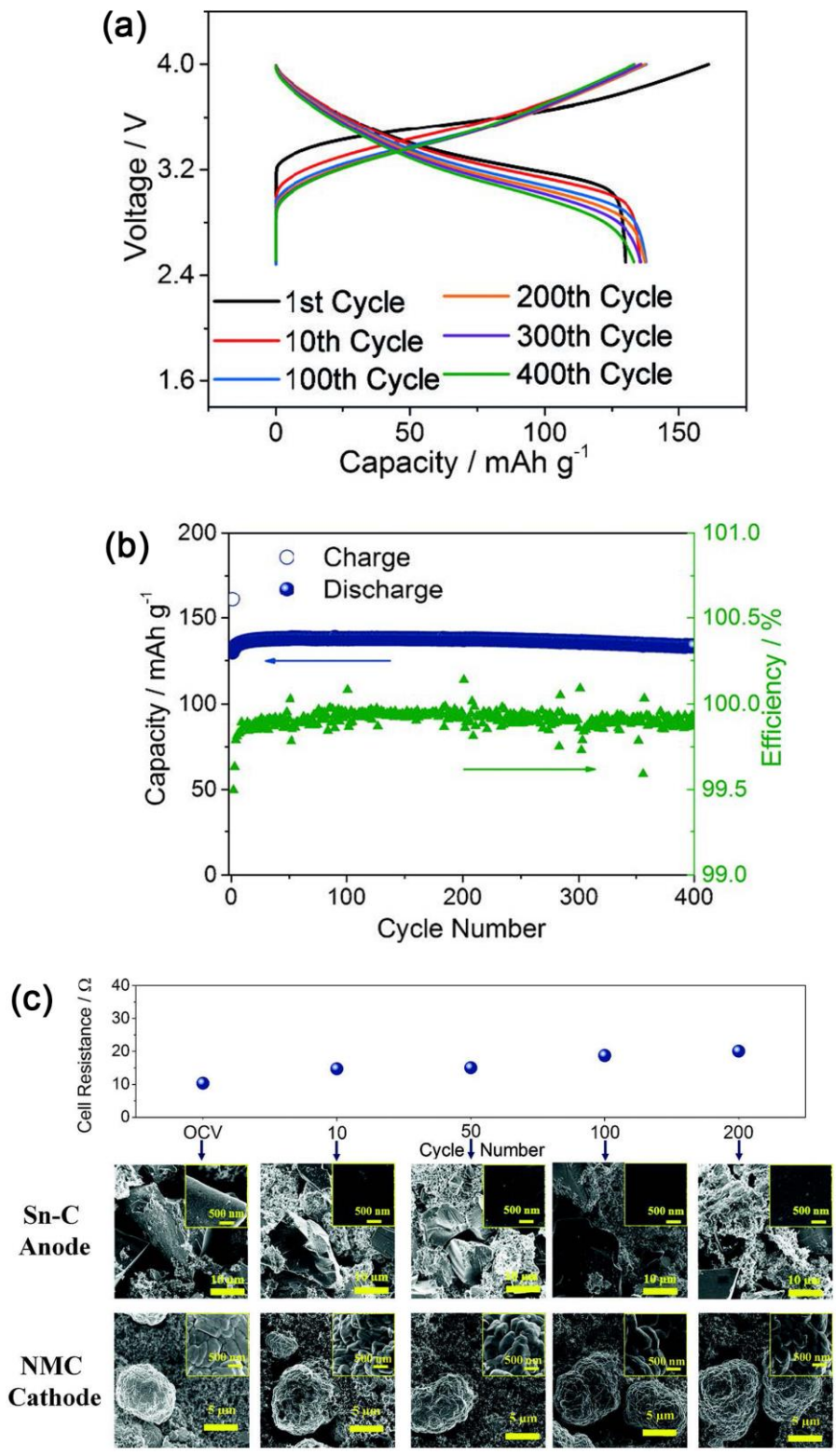


Figure 3

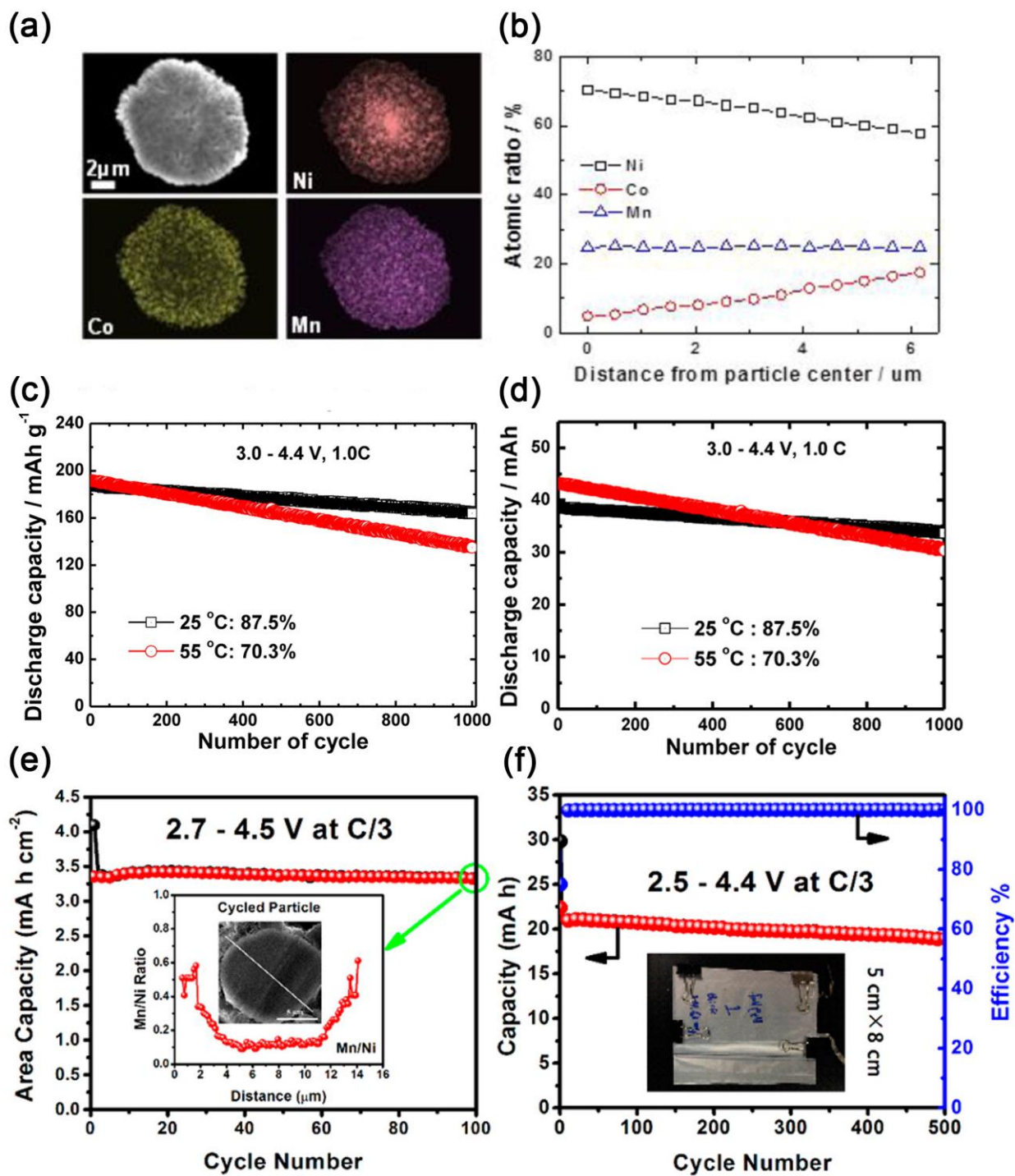


Figure 4

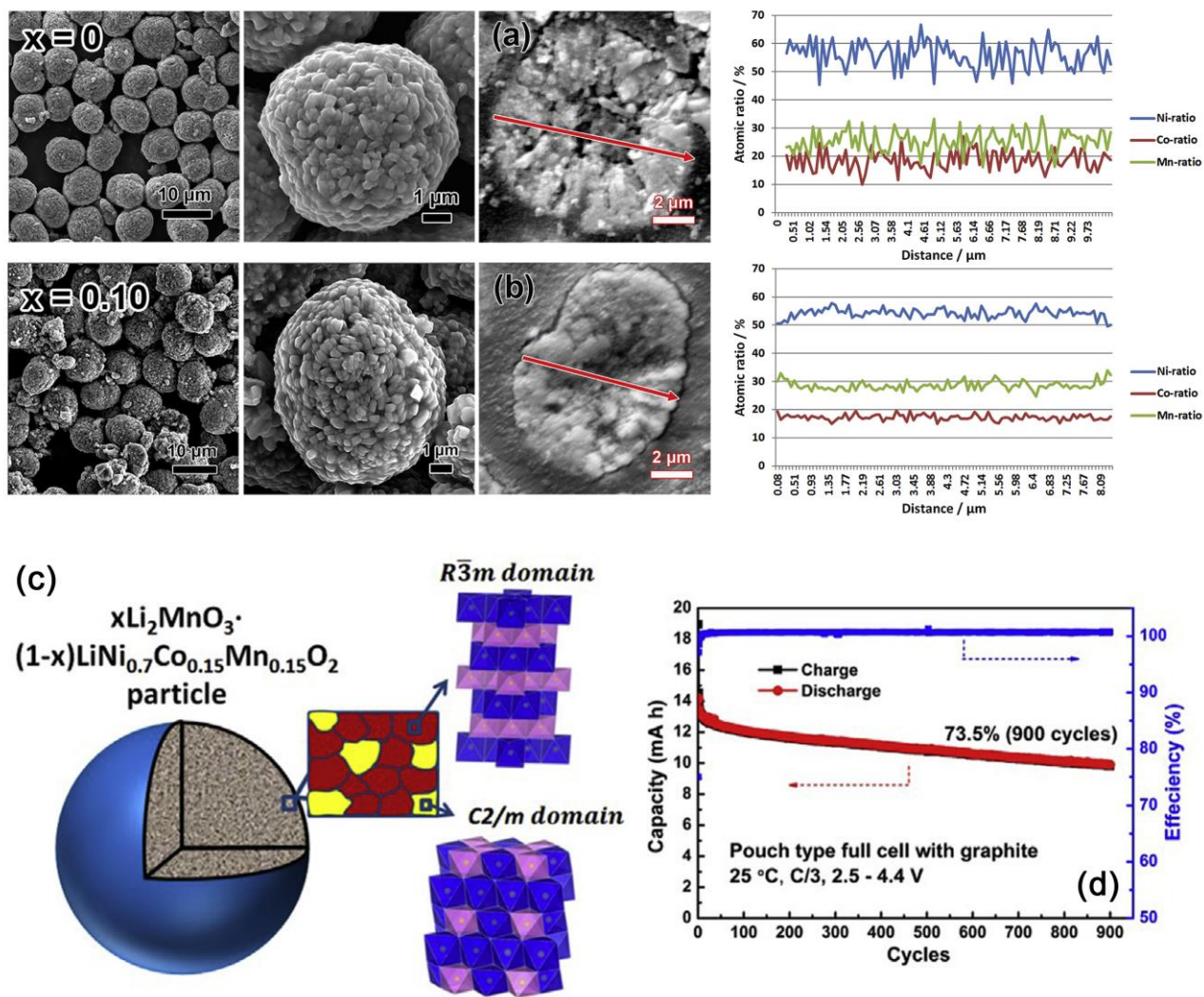


Figure 5

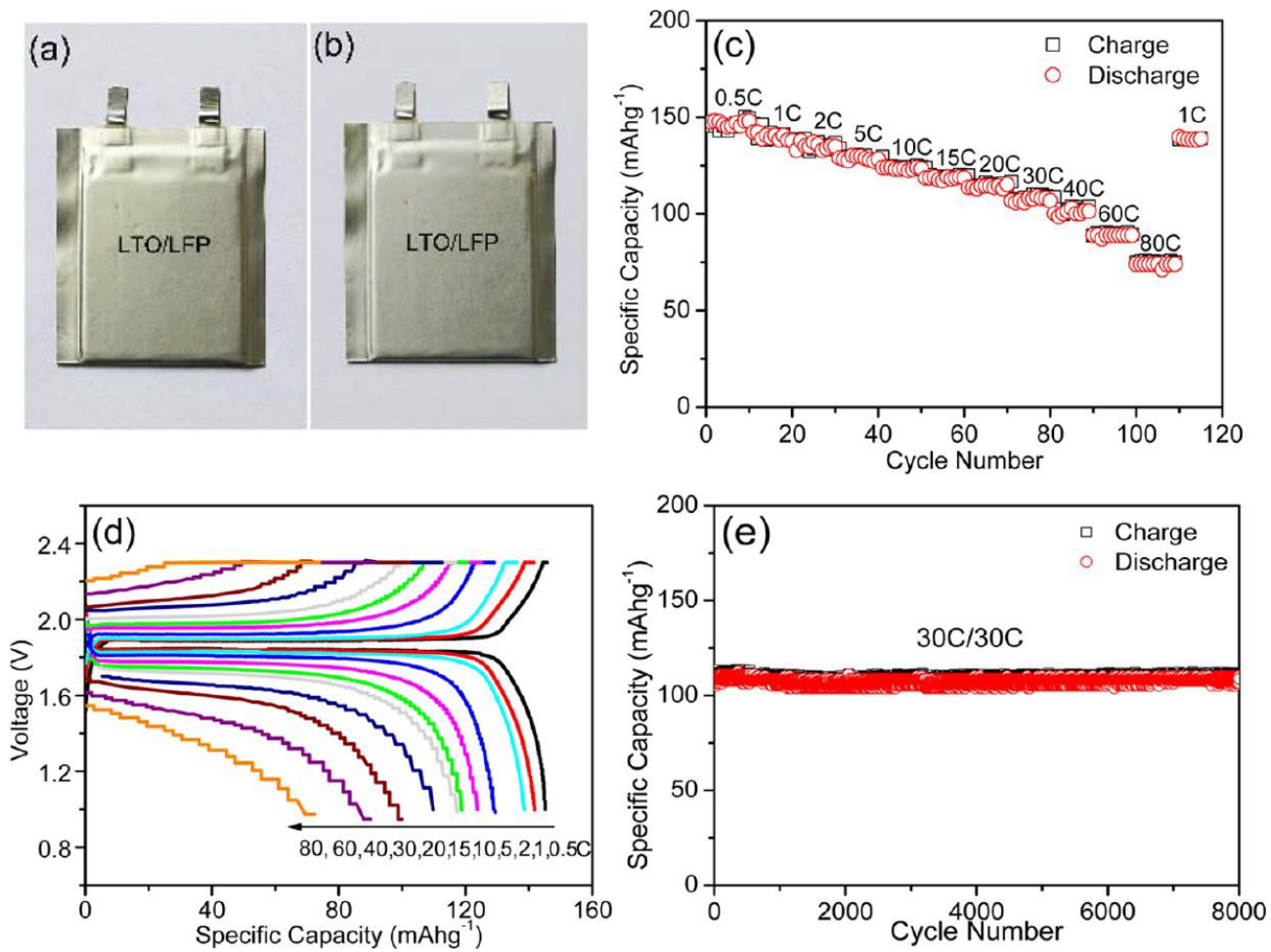


Figure 6

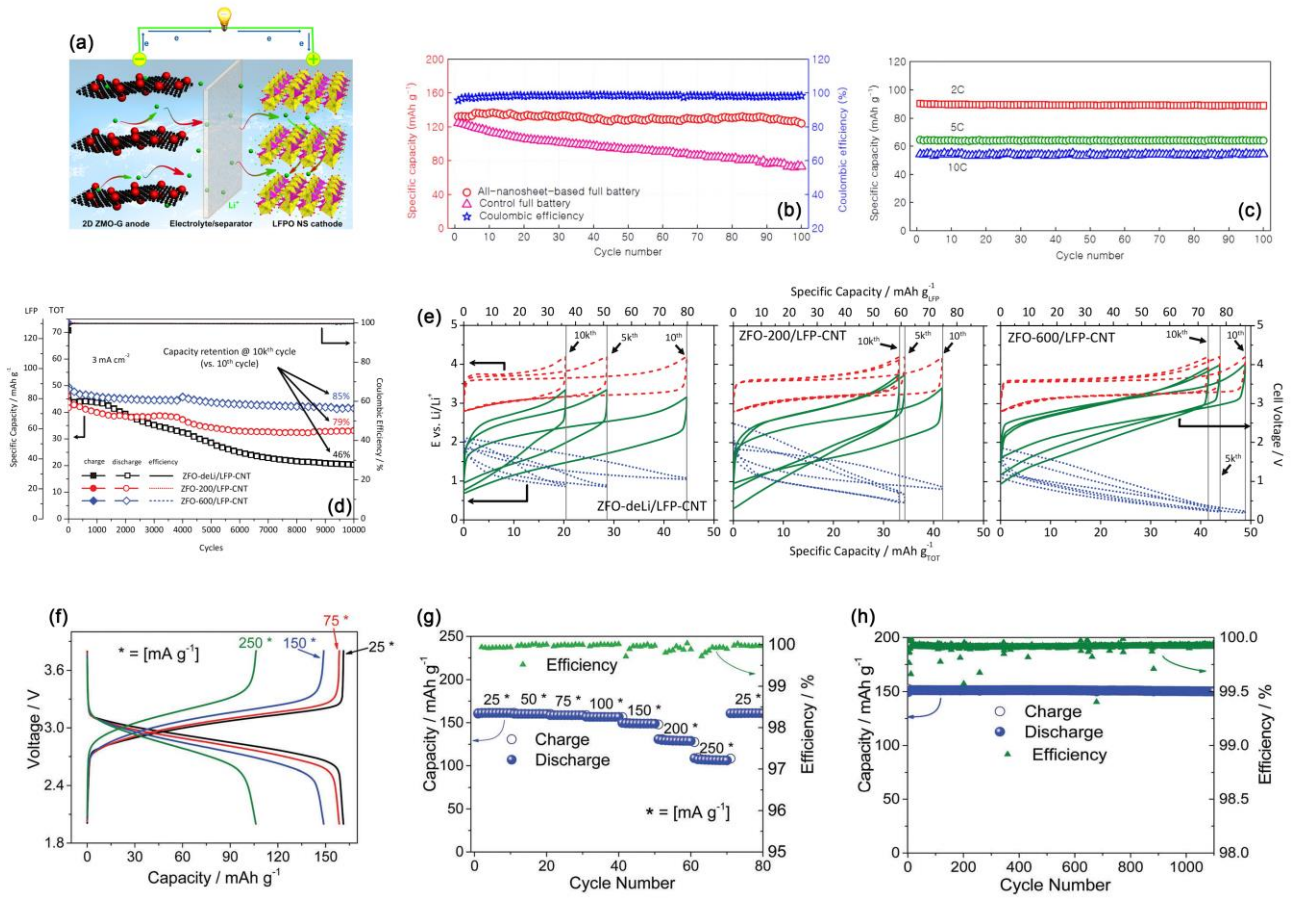


Figure 7

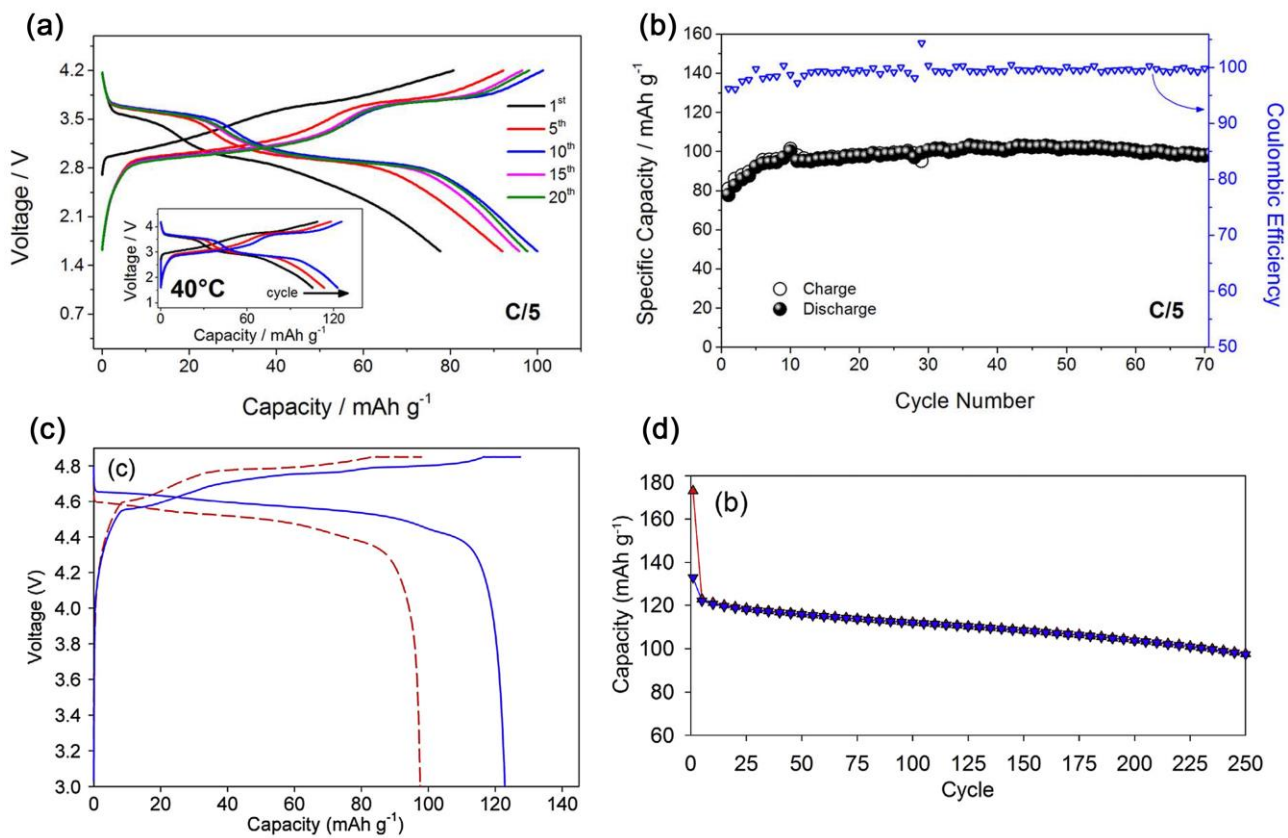


Figure 8

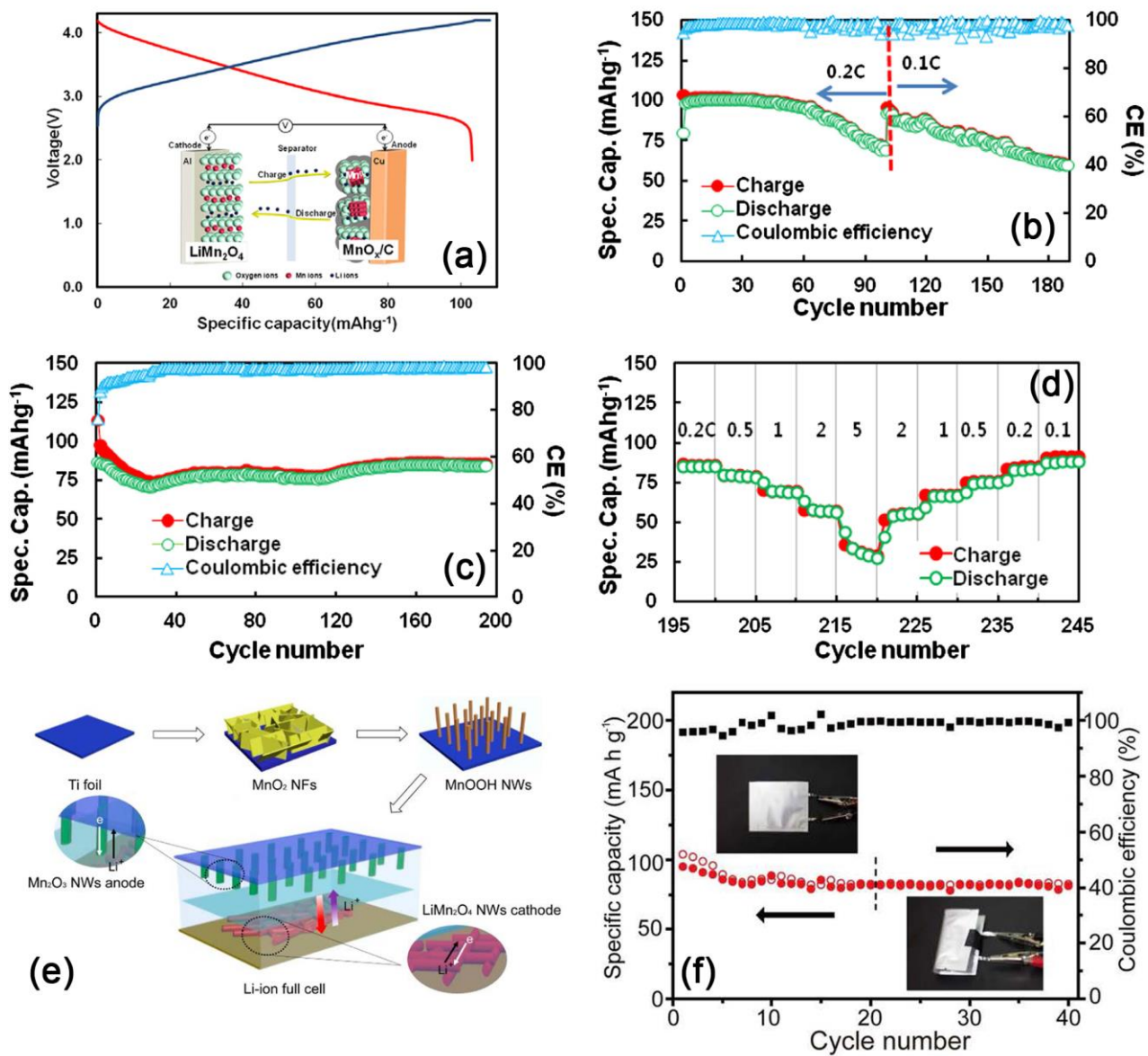


Figure 9

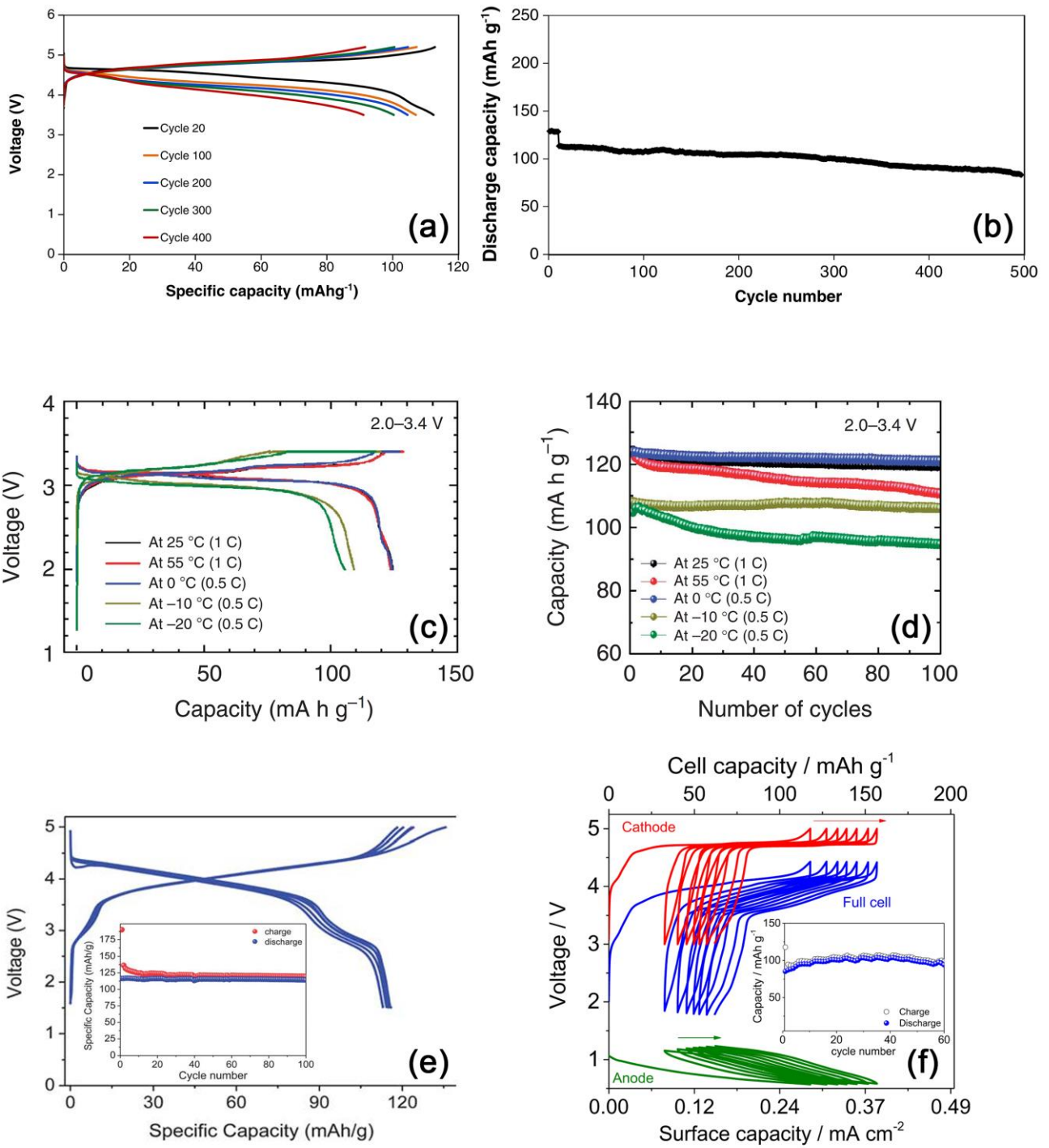


Figure 10

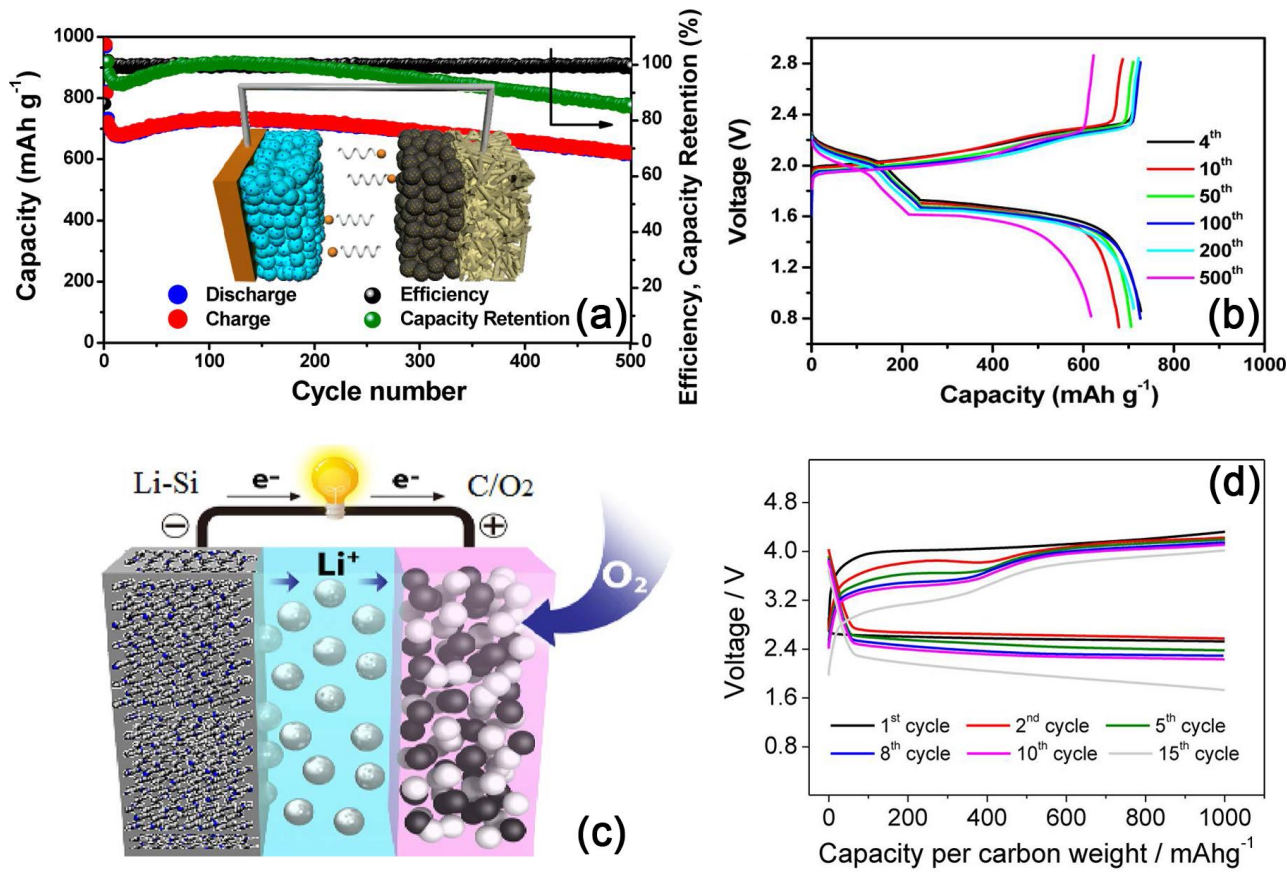


Figure 11